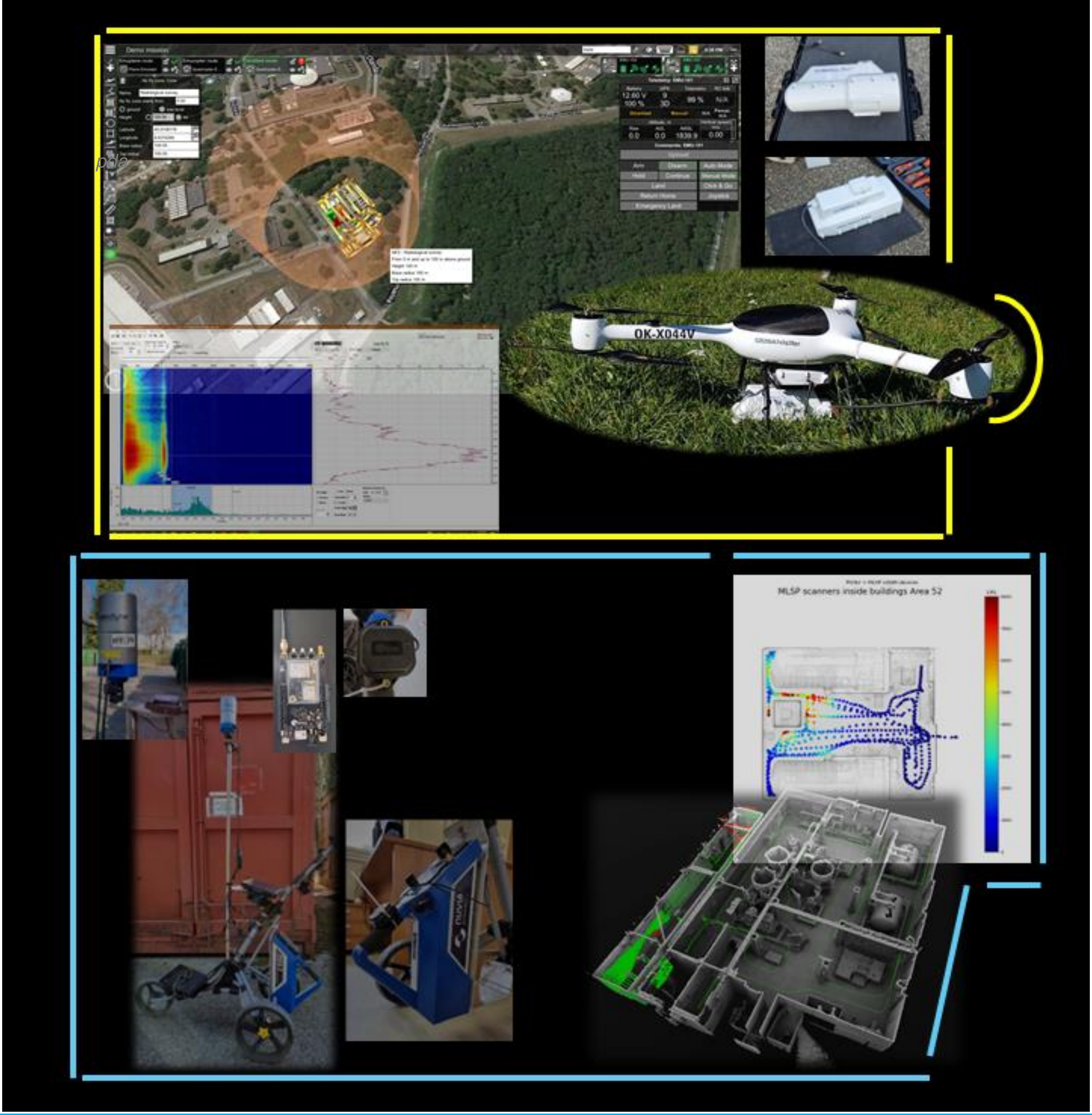

Advanced technologies for radiological characterisation by automatic and semi-automatic nuclear instrumentation

CASE STUDY

KP-JRC-008

29/05/2024

Cover photo

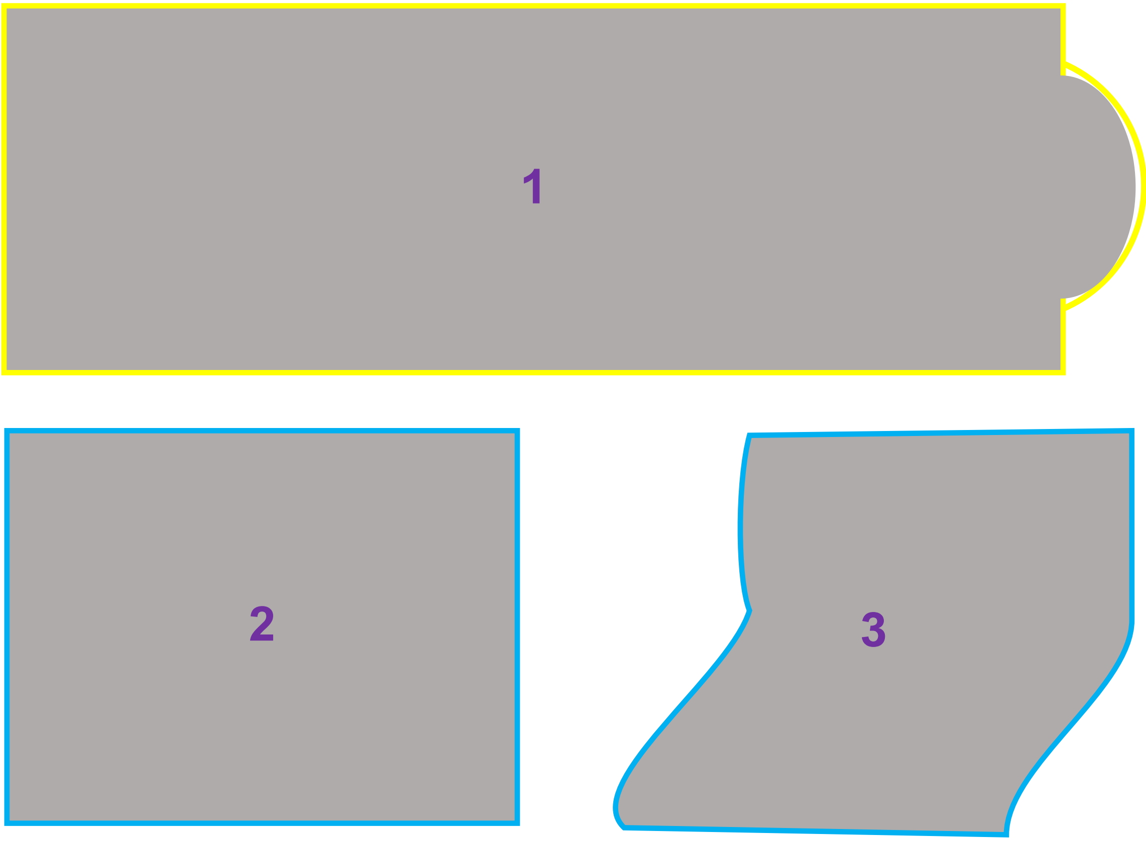

1. UAS in the field: (clockwise) a. flight planner software; b. NaI gamma & neutron detector; c. UAV, d. Gamma spectra analyser software.

2. A coupled system with a GNSS or LiDAR device associated with a Radioisotope Indentifinder: (clockwise) a. LiDAR scanner; b. GNSS receiver; c. GNSS antenna; d. RIID; e. a completed system on field.

3. A LiDAR and nuclear device on inside area. (Top) A sample of geo-localized radiological measurement inside a building; (Bottom) Cloud view of the scanned area with a LiDAR.

CREDITS

EDITORIAL NOTE

This publication has been prepared from the original material as submitted by the contributors and has not been edited by the author. The views expressed remain the responsibility of the contributors and do not necessarily represent the views of the EC-JRC.

This publication does not address questions of responsibility, legal or otherwise, for acts or omissions on the part of any person. The mention of names of specific companies or products (whether or not indicated as registered) does not imply any intention to infringe proprietary rights, nor should it be construed as an endorsement or recommendation on the part of the author.

The author has no responsibility for the persistence or accuracy of URLs for external or third-party Internet web sites referred to in this publication and does not guarantee that any content on such web sites is, or will remain, accurate or appropriate.

Foreword

In 2021, the European Commission (EC) adopted a new proposal for a Council Regulation[1] establishing a dedicated financial programme for decommissioning nuclear facilities and managing radioactive waste. This instrument covers the co-funding of the decommissioning programmes of Bulgaria, Slovakia, and the decommissioning of the Joint Research Centre (JRC). A separate Council Regulation[2] was adopted for the decommissioning programme of Lithuania.

The EC JRC is mandated to foster the spread of decommissioning knowledge across all the European Union Member States and facilitate knowledge sharing arising from implementing the abovementioned decommissioning programmes, funded by the Nuclear Decommissioning Assistance Programme (NDAP).

The decommissioning operators from the NDAP (NDAP Operators) implemented and tested a knowledge management methodology in 2021 through Project ENER/D2/2020-273. Using this methodology, the NDAP Operators can develop Knowledge Products that are currently available to share with other European stakeholders. In addition, this methodology is under implementation in the JRC Nuclear Decommissioning and Waste Management Directorate (NDWMD), which becomes a knowledge generator extracting the knowledge from the ongoing decommissioning activities at the different sites (Geel, Ispra, Karlsruhe, and Petten).

The JRC NDWMD aims to become a Centre of Excellence in nuclear decommissioning knowledge management and develop a decommissioning knowledge platform which allows exchanging information and building on the best practices in the EU inside the multi-annual financial framework (2021 – 2027) strategy. The operational phase of the project is expected to start in 2024 to develop ties and exchanges among EU stakeholders and document explicit knowledge and make it available through multi-lateral knowledge transfers on decommissioning and waste management governance issues, managerial best practices, technological challenges, and decommissioning processes at both operational and organisational level, to develop potential EU synergies.

This is a Knowledge Product prepared by Despe-Vuje for the JRC NDWMD.

Document code	KP-JRC-008		
Performed by	Francesco Raiola		
Revised by	Nuclear Decommissioning Knowledge Management Team		
Version	V0	28-Feb-24	Initial version
	V1	17-May-24	Review version
	V2	11-Jul-24	Final version
Sent to	Andrea PIAGENTINI		
Approved by	Andrea PIAGENTINI		

[1] Council Regulation (Euratom) 2021/100 of 25 January 2021 establishing a dedicated financial programme for the decommissioning of nuclear facilities and the management of radioactive waste, and repealing Regulation (Euratom) No 1368/2013.

[2] Council Regulation (EU) 2021/101 of 25 January 2021 establishing the nuclear decommissioning assistance programme of the Ignalina nuclear power plant in Lithuania and repealing Regulation (EU) No 1369/2013.

PRODUCT DESCRIPTION

The *Advanced technologies for radiological characterisation by automatic and semi-automatic nuclear* instrumentation report was prepared by a team of experts from NUVIA Process at JRC-ISPRA Unit G.III.9 (current Unit J.002) in Italy. The product conveys the experience gained during the execution of a Pilot Project on Contaminated Soil Management under the Nuclear Facilities Decommissioning and Support to Operations Framework Contract (NFD&SO) at EC-JRC between the years 2021 and 2022.

The two case studies presented in this report aim to assist operator personnel in familiarizing with different automatic and semi-automatic procedures for nuclear facility characterization and for the subsequent clean-up with the use of different nuclear radio-identification technologies.

One case will assure also be suitable for a facility radiation survey, which is the final radiological characterisation survey of the facility and site following the completion of decommissioning to ensure the end state for the facility has been achieved.

ABSTRACT

This product provides decommissioning and waste management organisations with insights and experience in the selection and use of technologies for facility characterization. Some technologies can reduce the time impact and improve the quality of certain activities by minimising personnel to perform it to increase safety. It will describe the different type of nuclear detection system in use and especially the ones tested on field. It will show the importance of the correct expert use of advanced technologies but at the same time the flexibility due to the specific condition. Two case studies will be analysed for radiological characterization measurement coupled with a dedicated GNSS or phone base localization system in outdoor and indoor environment.

The two case studied will also provide an example of applying modern semi-automatic and automatic system to perform a radiological characterization with the assistance of robotic system.

This document will not be able to cover of all available technologies for characterization of a site or a facility but it will provide the sources of information and tips that could help the user to take the “right” decision.

OBJECTIVE

This Knowledge Products aims to provide an example of evaluating and choosing the automatic or semiautomatic nuclear and radiological technologies to perform a facility characterisation or site characterisation. Secondly, the case studies to show the decision-making process to perform a specific procedure with a set of requirements based on the specificity of the nuclear facility in analysis. The last objective of this product is to consider the cost-effectiveness of using an automatic and/or semi-automatic system to perform the characterisation tasks.

APPROACH

The project team incorporated experiences from soil and facility characterisation in decommissioned nuclear power plants, as well as experience from testing radioisotopes nuclear devices for Nuclear Security, Safety and Safeguards Unit G.II.7 at JRC Ispra into developing these case studies. They also integrated results from past projects exploring innovative and advanced technologies for the radiological characterisation of facilities and soil in large areas.

RESULTS, FINDINGS, AND INSIGHTS

This report will permit a comprehensive evaluation of using a semi-automatic and/or automatic system to perform radiological characterisation of nuclear facilities and soil ground. The nuclear operator will acquire specific knowledge on the authorising process for using an Unmanned Aerial Vehicle (aka drone) and the technical procedure to evaluate the specific limitations of different case studies in analysis. It will also provide tips for performing a quality radiological measurement and the limitations of using those technologies in particular environments or facility size and complexity. It will be provided with analysis software suggestions regarding their facility size and building complexity. It will provide tips on the software complexity for a flight planner's determination.

These results will not favour one specific company, but they will only be focused on the type and characteristics of each used technology, as this is not a performance test.

TARGET USERS

The report shows that those advanced technologies require tasks not present in a current nuclear operator's job duties, thus requiring an ad-hoc training course on radioisotope identifier devices and UAV piloting. A new professional figure in nuclear decommissioning or a professional figure who, as a ‘young’ operator, might be willing to initiate his/her career.

Of course, a possibility is to employ outside contractor that are specialized in UAV piloting and tandem them with a nuclear operator and a radioprotection officer/engineer to precisely define the technical procedure to be applied on specific cases.

APPLICATION, VALUE, AND USE

JRC-Ispra is progressing its Decommissioning & Waste Management Programme which encompasses complete immediate decommissioning of shut-down nuclear installations on site and the conditioning and temporary storage of associated radioactive waste, either new waste from the decommissioning activities or historic waste from past operation of the facilities. One of such waste streams is (potentially) contaminated soil or other types of surfaces such as asphalt or cement.

Radiological surveys of soil and other types of surfaces have been carried out in JRC-Ispra facilities, in particular in the INE Complex, in Area 40 and in the old Liquid Radioactive Waste Treatment Station, STRRL considering **outside** and **inside** areas. This document highlighting the areas for improvement and development of technologies and techniques underpinning the activities of soil (and floor) remediation process and their real-life testing. Such new innovative technologies may bring a lot of savings in the contaminated soil and floor management projects carried out at the end of dismantling projects at nuclear facilities.. This knowledge product gathers various technologies in use for radiological survey inside and outside area and associated tests in-field. The market of automation has showed a fast-pacing evolution and creativity with use of different form of automatism (arms, vehicle, mini boat. mini sub, UAV, quadruped system and more) but they have been facing always the cost, the specific of the tasks and the disruption of the electronics in high radiation zones. This product could show to the users that also commercial automate or semi-automate system could provide an improvement on efficiency, cost and adaptability on different condition.

As an example of an already functioning system is the SIGMA Network. They have been successfully deployed a networked radiological protection system by UAV, vehicle, robot, in cities and with security forces in varying operations: urban, tactical and event-based scenarios and in small reality like a NPP site.

One can consider deploying several automatic and semi-automatic nuclear devices for different purposes that can be categorized as for static or dynamic measurements in **outside** or **inside** area.

Then, the radiological data collected is securely stored in a network cloud system, hosted by one of the major company cloud system (like AWS, Microsoft Azure, GCP account for 65% of the global cloud infrastructure market source Statista.com) or by a private company network. All data is then ready and available for the specific purpose in study for a decommissioning plan of certain facilities.

Besides, this interconnected radiological characterisation network system could provide:

- A cost-effective, continuous radiation reporting from radiation detectors that are part of the network.
- A system that can cover cities, places of special interest or whole regions or a NPP site.
- A real-time radiation mapping with alerts.
- A historical radiological evolution of a nuclear site.
- A wide base knowledge on facility characterization.

KEYWORDS

Knowledge management decommissioning; Facility characterization;GNSS;LiDAR;UAS;decommissioning

TABLE OF CONTENTS

LIST OF ACRONYMS AND DEFINITIONS

AWS	Amazon Web Service
CPS or cps	Counts per seconds
CSV	Comma-separated values
Despe/Vuje	Joint Despe S.a.s. and Vuje
ENAC	Ente Nazionale per l'Aviazione Civile (Italian Authority for Civil Aviation)
ENAV	Italian Air Navigation Service provider
FOV	Field of View
FWC	FrameWork Contract
GCP	Google Cloud Platform
GLONASS	GLObalnaya NAvigatsionnaya Sputnikovaya Sistema in Russian
GNSS	Global Navigation Satellite System
GI	Gamma Imager
INE	Impianto Nucleare ESSOR (Nuclear Power Plant ESSOR)
JRC	Joint Research Centre
JRC.J.1	Ispra Operational Nuclear Decommissioning & Waste Management Unit
LCSR	Laboratorio Caldo Studi e Ricerche (Hot-cell Research Facility)
LiDAR	Light Detection and Ranging
MLSP	Mobile Laser Scanning Platform
MTOW	Maximum Take-off Weight
NDA	Non-Destructive Analysis
NPC	NUVIA ProCess
POI	Point of Interest
RIID	Radiological Isotopes Identification Device
RINEX	Receiver INdependent Exchange format
RPAV	Remoted Piloted Aerial Vehicles
SC	Specific Contract
SORA	Specific Operations Risk Assessment
STeAM	Sensor Tracking and Mapping
STRRL	Stazione di Trattamento di Rifiuti Liquidi
UAS	Unmanned Aircraft System
UAV	Unmanned Aircraft Vehicle
VLOS	Visual Line of Sight

LIST OF FIGURES

LIST OF TABLES

1. BACKGROUND

In the frame of SC59 – *Pilot project on contaminated soil management* - and SC68 - *Safe conservation, post-operational clean out and pre-decommissioning support service to INE nuclear plant and LCSR hot-cells facility* – the team performed a series of radiological measurements outside and inside buildings using a geo-localization system for radiological measurement in dynamic and static mode. The SC59 [1] was a Pilot Project dedicated to the field of innovative digital technologies applied to the management of contaminated or potentially contaminated soil and floors as part of the Innovative Technologies Integration (ITI) Sector. This team was in charge of holding the innovative technologies watch, managing Pilot Projects that support innovation integration into nuclear decommissioning and contributing to knowledge dissemination.

The SC68 [2] pertains the activities supporting the safe conservation, post operational clean out and pre-decommissioning in the INE (Nuclear Power Plant ESSOR) and the LCSR (Hot-cell research facility). In the framework of this contract, the contractor applied a radiological measurement campaign, using a specialized innovative radiological device, to provide a radiological survey to test the performance (quality assessment) of this technology on some INE and LCSR area as inputs for subsequent activities in safe conservation, post operational clean out and pre-decommissioning.

This report will be divided in two specific case studies:

1. Dynamic radiological geo-localized measurement in **outside** environment using radioisotopes identifier devices
2. Dynamic and static radiological geo-localized measurement in **inside** environment using radioisotopes identifier devices

The first case consists of radiological measurements with GNSS (Global Navigation Satellite Systems) equipment (several type of combination GNSS receivers + antenna) and the NuHLS-100, a nuclear NaI (Sodium Iodide detector) portable detector for a set of dynamic radiological measurements in Stazione di Trattamento di Rifiuti Liquidi (STRRL site). It will also include a radiological aerial survey with an Unmanned Aircraft system (UAS) from the contractor, consisted of a UAV (BRUS-H), a payload (DRONE-G) and a ground control system.

The second case consists of radiological measurements in Impianto Nucleare ESSOR (INE) and LCSR hot-cells facility with the use of NuVISION gamma camera (aka GI o gamma camera), gamma radiation detector with *Compton imaging* and coding *mask* technologies. It will also include the radiological measurement in STRRL on building 52 and 52A with the use of NuHLS-100, a standalone radiometric system, and a Mobile Laser Scanning Platform (MLSP) LiDAR for localization with laser scanning.

1.1. Challenges

The two case studies present different challenges and novelty with them. Both show the complexities applying a new system for radiological characterisation that has been never performed before by a radioprotection officer (as usually with a standard NaI portable radioisotopes device). The two case studies combine the different scopes of the two projects but have in common the need to prove or demonstrate the use of innovative technologies to perform a radiological characterization with an automatic or semi-automatic system coupled with the geo-localization of the radiological measurements.

In both cases, a pre-assessment of the measurement condition by an expert on nuclear measurements was essential for the outcome of those radiological measurements.

One can summarize in short the following challenges:

Advanced technologies for radiological characterisation by automatic and semi-automatic nuclear instrumentation

- Choose the correct nuclear detectors and geo-localisation system for the scope;
- Acquire the proper technical knowledge in the nuclear operator team to perform the measurements in two different environments: **inside** and **outside** a facility or area;
- Define the timeframe to acquire enough data for the measurement campaign and optimize the cost of the equipment.

1.2. Constraints

Due to the innovative aspects of the technologies the main constrains were in the creation of a specific work procedure that was limited by the followings:

In particular, recorded data from a report on 2016 radiological measurements [3] were performed in very different conditions and with different nuclear detector efficiencies by using a $50\ x\ 100\ x\ 5\ cm$ plastic scintillator and 3" NaI gamma ray spectrometer detector of well-known capabilities. Those data were used as a base for the assessment of the possibility to apply new advanced technologies and with the goal in mind to demonstrate that there are in place new radiological scanning system that they can perform with faster and more accurate way with adding capabilities in term of geo-localization and 3D representation of the scanned area..

This Knowledge Products aims to provide an example of evaluating and choosing the automatic or semi-automatic nuclear and radiological technologies to perform a facility characterisation or site characterisation. Secondly, the case studies to show the decision-making process to perform a specific procedure that required a set of requirements based on the specificity of the nuclear facility in analysis. The last objective of this product is to consider the cost-effectiveness of using an automatic and/or semi-automatic system to perform the characterisation tasks.

Taking in account these condition that following two case studies are to be taken as a quality assessment of these innovative technologies and suggestion or guidelines will be indicate (i.e. a Tips box) clearly for the two case studies.

1.3. Relevance

This knowledge product produces some measurable facts that are quantified within reasonable and valuable errors based on the statistics of the model applied. Then those provide the base line for the determination of a quality assessment these automatic and semi-automatic nuclear technologies, like operator safety, data acquisition time, man-days, operational cost and etc. At the same time, they revealed their limitation due to their development phase as a new technologies.

This knowledge product will potentially contribute to reducing the cost and improving the organization of a measurement campaign by reducing the labour involvement during the automatic and semi-automatic operations. An initial radiological assessment could be performed on facility characterization that in a short time will produce a detailed quality radiological map of the involved area.

It could potentially of high Impact on Performance as level up to 5 as in the Termination of authorization → Final radioactivity survey where an aerial radiological geo-localized survey could be deemed.

The input data upon which this knowledge product is built are part of practical examples of R&D on the decommissioning facilities using innovative technologies. For their intrinsic characteristic, they potentially significantly impact the work of the radioprotection team, or the contractor involved in the characterisation. The innovative technical solutions used in those case studies are based on very specific technical knowledge that required a collaboration of other professional figures that could not be part of or implemented in a nuclear decommissioning plan. An organisation that uses R&D in their organigram will definitely benefit from this knowledge product.

The nuclear industry is not new to robotic systems that are mostly focused on mechanical arms, manipulators, crawlers and climbers, Underwater Remotely Operated Vehicles, and others. This knowledge product shows a radiological survey by an autonomous system and geo-localized indoor by a 3D laser scanner coupled with a RIID.

The methods described are relatively new and still not routinely deployed in decommissioning projects.

2. SCOPE

The analysis of the different cases brought the operator to address the specific positive and negative outcome of automatic or semi-automatic system technologies. The specifics will be analysed in the following:

1. Cost-effective in using them;
2. Time-saving on the operation for characterisation;
3. Accuracy and quality of the data;
4. Safety procedures applied;
5. Procedure scheme simplicity and/or novelty in these nuclear technologies.

3. OVERVIEW OF THE CASE STUDIES

The two case studies can be briefly summarized as follows:

Case Study #1 – Dynamic radiological geo-localized measurement in **outside** environment using radioisotopes identifier devices.

Case Study #2 – Dynamic and static radiological geo-localized measurement in **inside** environment using radioisotopes identifier devices.

The case studies are described in detail in Sections §4.1-4.6 and §5.1- [4], [5], [6], [7], [8] of this report. Each case study is structured as follows (when a section is deemed necessary):

- Sources of information used to develop the case study
- Description of activity and process
- Regulatory & Licensing aspects
- Quality aspects and data
- Findings, results
- Potential Benefits for Other Organizations

4. CASE STUDY No.1

4.1. Sources of information

This case required the collection of many sources of information that are used to define or acquire the followings:

- Acquisition of the permit to fly over the JRC-Ispra area - EASA regulations (In compliance with EU Regulations 2019/947 and 2019/945 and relative NOTAM) [9], [10]
- STRLL acquired radiological data on previous campaign [3]
- Define the area of operation for the data acquisition in Area 52 - AREA 52 Planimetria [11]
- Define the structures above a certain level from the ground – Cisterna Esterna in Area 52 [12]
- Technical documentation on radiological survey with UAS and GNSS geo-localization [5] [6]
- Characterisation plan of the JRC-Ispra facilities - DECOMMISSIONING PLAN [13]
- IAEA nuclear safety and security glossary - [14]
- IAEA guidelines for radioelement mapping using gamma ray spectrometry data - [15]
- ANSI and IEC standard on handheld nuclear devices

In particular, the STRRL Land Area Characterization Survey Report [3] presents the results of a radiological survey conducted at the STRRL (area 52) facility at the Joint Research Centre (JRC) in Ispra. The radiological survey aimed to identify the radiological status of the ground/soil and roads of the STRRL area using the NuHLS GHV 1000 (POLARIS) (in the 2016 campaign) and NuHLS GHP 100 (PGIS or NuHLS100) instruments. The survey found that a significant portion of the measured count rates were influenced by external radiation sources, such as tanks and drums containing radioactive wastes. The background value fluctuated, making it impossible to calculate a net count rate and, consequently, the ^{137}Cs equivalent specific surface activity.

Ten areas of interest were identified as having significantly higher count rates and should be further investigated using means that can isolate the measured signal coming from the ground. A source coding methodology was tested to estimate whether the higher count rates were due to contamination or not, but the results suggest this methodology may not be reliable enough for such inferences. The report recommends conducting collimated surface spectrometry measurements and ambient dose-rate surveys in these areas and, if necessary, analysing soil samples at different depths to establish if the higher measured count rates are due to contamination.

[1] NE.45.2253.A.001 Rev.0: SCTS - Contaminated Soil Management

[2] NE.67.2549.A.010 Rev.2 – AREA 52 Planimetria

[3] 114041_SC59_PR 07 Rev.0 - Procedura di caratterizzazione radiologica geolocalizzata all'interno degli edifici in STRRL

[4] 114041_SC59_NT 07 Rev.0 - Dynamic GNSS Geolocalisation of a Radiological Survey in Area 52

[5] Carlos Sánchez, Pierluigi Taddei, Simone Ceriani, Erik Wolfart, Vítor Sequeira, Localization and tracking in known large environments using portable real-time 3D sensors, Computer Vision and Image Understanding, Volume 149, 2016, Pages 197-208

[6] C. Sanchez-Belenguer, E. Wolfart, A. Casado-Coscolla and V. Sequeira, "RISEdb: a Novel Indoor Localization Dataset," *2020 25th International Conference on Pattern Recognition (ICPR)*, 2021, pp. 9514-9521, doi: 10.1109/ICPR48806.2021.9413258.

4.2. Case Study Description

At the JRC-Ispra in the STRRL – Stazione di Trattamento di Rifiuti Liquidi, often referred to as Area 52, in the frame of the specific contract SC59 and as part §4 of it - *Geolocation and Mapping* [1], [16] – an expert team performed radiological geo-localized measurements with the following technologies in the outside environment by an automatic and semi-automatic system:

1. GNSS (Global Navigation Satellite Systems) equipment coupled with the NuHLS-100 contractor instruments (aka PGIS), a nuclear NaI portable detector for a set of dynamic radiological measurements.
2. An Unmanned Aircraft system (UAS) from contractor coupled with BRUS-H payload (DRONE-G) consisted of an interchangeable set of two nuclear detectors: a plastic scintillator 1L and a NaI 3"x3".

For both dynamic measurements in an outside environment, the work procedure was the followings:

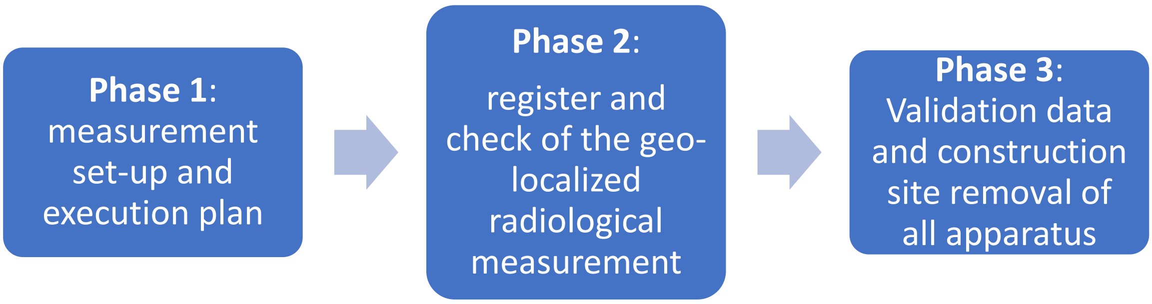

On March 2022, a 2 days geo-localized radiological measurements were undertaken in outside area of STRRL, in accordance with the Area 52 planimetry [11], [12]. The main objective of these measurements was to identify the state of the art and innovative technologies for geo-location of radioactivity measurements and to test them in full-scale project conditions coupled with a radioisotopes identifier instrument (aka RIID).

The paths for the radiological measurements coupled with a GNSS (Global Navigation Satellite System) system are based on the planimetry of the Area 52 and of the buildings/tanks/structures in the area of interest. For the dynamic GPS radiological measurements in outside environment, the area has been divided, for convenience, in three sections (A, B and C) and three B-subsections as seen in Figure 1, on the right, the underlined coloured picture shows the radiological data from Contaminated soil Management [16]:

1) Sec. A – green zone in the Figure 1 and A1 point of background for the PGIS-2
2) Sec. B – critical zone inside the controlled zone

    a) B1 – orange zone
    b) B2 – violet zone
    c) B3 – dark green zone
3) Sec. C1 – blue zone

Figure 1: *(On the left) Google map of the STRRL area of interest (red line) and around it (yellow path). (On the right) Map of the analysed sections A, B and C subject to the dynamic GPS measurements. Indicate also the A1 background point (red point) for the radiological detector (source Google Map).*

To perform this field measurement the team used the following instrumentations for radiometric and geo-localization recorded data (see Figure 2 - Figure 4 and Table 7 - Table 1):

1. NuHLS-100 (aka PGIS-2 or RIID[3]) nuclear detector with NaI(Tl) crystal ($0.347\ litres$);
2. U-blox C099-F9P-1-03 development kit equipped with a ZED F9P receiver with dual-frequency capabilities (aka Ublox);
3. U-blox EVK-M8U, an evaluation kit equipped with a U-blox M8U receiver integrating inertial sensors;
4. BEITIAN BT-200 antenna capable of covering all GNSS bands.
5. Several Android phones (Xiaomi Mi8, Xiaomi MiX, Samsung S21 Pro and Samsung S20 FE) able to provide GNSS raw measurements.
6. The technical characteristics of the NuHLS-100 and U-blox C099-F9P-1-03 are showed in the Table 7. The U-blox EVK-M8U has similar characteristics of its relative C099, then it's not indicated.

The PGIS-2 and the Android phones operate using their integrated GNSS antenna, whereas the two U-blox devices are connected to an external antenna to improve the receiver performance.

[3] Radioisotope Identifier Device

The C099-F9P application board (see Table 7) allows efficient evaluation of ZED-F9P (receiver module). The U-blox ZED F9P receiver is a multi-constellation dual-frequency receiver able to process signals from GPS, Galileo (European global navigation system), GLONASS (GLObalnaya NAvigatsionnaya Sputnikovaya Sistema in Russian), and BeiDou (Chinese navigation satellite system). It also has an ANN-MB multi-band, high-precision GNSS antenna [12]. This antenna has a low form factor (see Figure 3 on the right) and can be easily mounted on the top of a stick to improve visibility conditions. This antenna has been used for most of the tests; a Radio Frequency (RF) splitter was used to provide its signal to both the U-blox ZED F9P integrated within the C099-F9P-1-03 development kit and the U-blox M8U receiver.

The U-Blox M8U is a single-frequency multi-constellation GNSS receiver processing GPS and GLONASS L1 signals. While this receiver does not feature the same capabilities, in terms of GNSS signal reception, the U-Blox ZED F9P it integrates inertial sensors (accelerometers and gyroscopes) that are used by the receiver to bridge GNSS data gaps [17]. Figure 4b provides a view of the EVK-M8U.

The U-center evaluation software provides a powerful platform for evaluating U-blox GNSS receivers. The software contains an NTRIP server/client, which can be used to manage the RTCM correction stream to and from a C099-F9P application board.

A second multi-frequency GNSS antenna, the BEITIAN BT-200 antenna (Beitian), was utilized for the tests. (see Figure 4c).

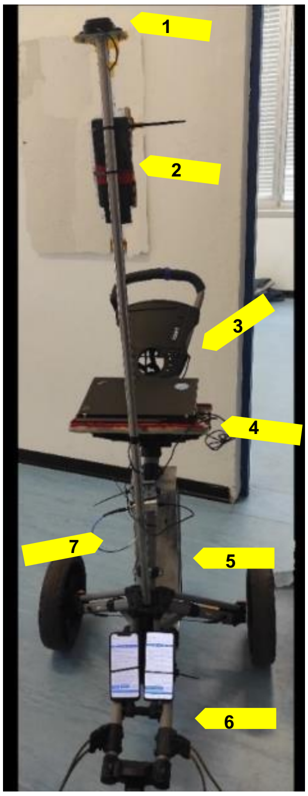

Figure 2: *(On the left) Full setup of in-field measurements in STRRL: 1. ANN-MB antenna; 2. S21 Ultra 5G; 3. U-blox F9P board (behind); 4. Laptop MS WIN OS; 5. PGIS-2; 6. MiX and Mi8 and 7. M8U Single frequency inertial receiver). (On the right) Instrumentation on the trolley in-field with the Beitian BT-200 antenna on the bottom.*

Figure 3: *From Left to right: NuHLS-100 radiological nuclear device, U-Blox C099-F9P-1-03 GNSS receiver and antenna.*

a. Extend antenna position

b. The EVK-M8U evaluation board integrating the U-blox M8U receive

c. Beitian BT-200 antenna

Figure 4: *Instrumentations for the field GNSS + radiological measurements in STRRL.*

To carry all the instrumentation a trolley (see Figure 5) was chosen and an external support was designed (see Figure 2, Figure 4 and Figure 5) by SketchUp Pro 2022 to adapt the NuHLS-100 to the laptop and the U-Blox system. The locations of the different devices were carefully selected to optimise signal reception. This was done considering the space constraints of the trolley. A vertical stick was welded to the trolley and used to support the receiver antenna. In this way, the antenna was placed at a relatively high position improving signal visibility. The PGIS-2 instrument was kept close to the terrain and far from the metallic trolley structure. Finally, the smartphones were placed in front of the trolley (see Figure 2). While this emplacement was not optimal, it was dictated by the space available on the trolley.

As it can be seen from Figure 2, the BEITIAN BT-200 antenna has a significantly larger form factor with respect to the ANN-MB U-Blox antenna. Thus, difficulties arose for fixing it to the top of the trolley stick.

The BEITIAN BT-200 antenna has a significantly larger form factor (see Figure 2 on the right). Then it was unfortunately placed at the bottom of the trolley. This solution was suboptimal and signal reception was penalized. For this reason, the ANN-MB U-blox antenna placed on top of the trolley stick was preferred and used for most of the tests.

Figure 5 shows the trolley set-up and the two attached structure: a) a plate to fix the PGIS-2 at the trolley at a lower position and b) a plate to support the laptop and the antenna. A later updated version was designed on the right side of the Figure 5. The two models separated and the improved plan was to build a shielding lead structure around the NuHLS-100 (aka PGIS-2) to optimise the position determination of the host-spot/s.

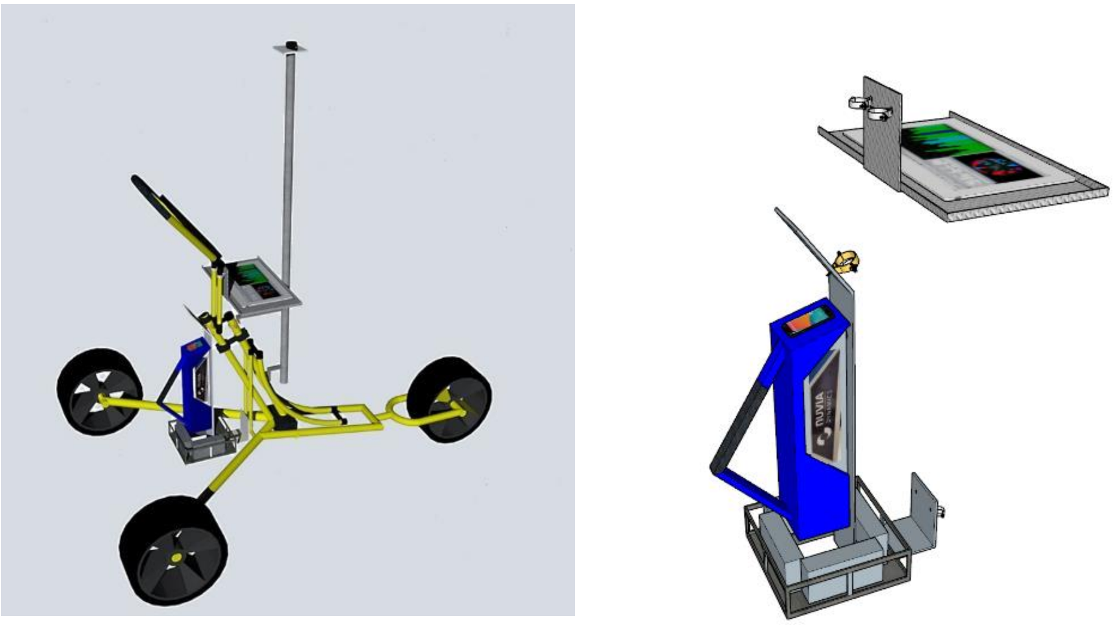

Figure 5: *(On the left) CAD drawing of the trolley. (On the right) CAD drawing of the metal laptop platform, PGIS-2 support and on the lower side a mock-up of Pb bricks structure for radiation shielding (source Sketch-up Pro 2022).*

> The effective solid angle of PGIS-2 is rather large due to the absence of a collimator in front of the crystal. Thus, it will be influenced by radiation background around it. Taking in account this limitation is extremely important during the radiological measurement.

The following QR code help to visualize in augmented reality (AR) the size of the PGIS-2 with a sample trolley (similar to the one used) to understand the real size of it to apply on your specific case and environment.

https://arknowledgeproduct .000webhostapp.com/ar/	The QR code on the left will give you access to an AR visualisation of the radiological device and its setup by using a phone or a tablet with a camera. It will help to visualize in a real environment the instrumentation (website 000webhostapp.com). Click on *Start AR KP WebXR* and tap on the phone screen to visualize it in your environment. Wait for loading the model.

The radiological data acquired from PGIS-2 (see RADaqLite manual [18] and *CustomROI.ini* in the detector configuration) are extracted by the PEIView software and converted into CSV format.

Before the extraction, the data are visualised with PEIView (DATAView software is part of the PEIView suite), analysed through the identification of the various photo-peaks of the radioisotopes of interest (i.e., Am-241, Cs-137, Co-60) and verified by the operator (see Figure 6).

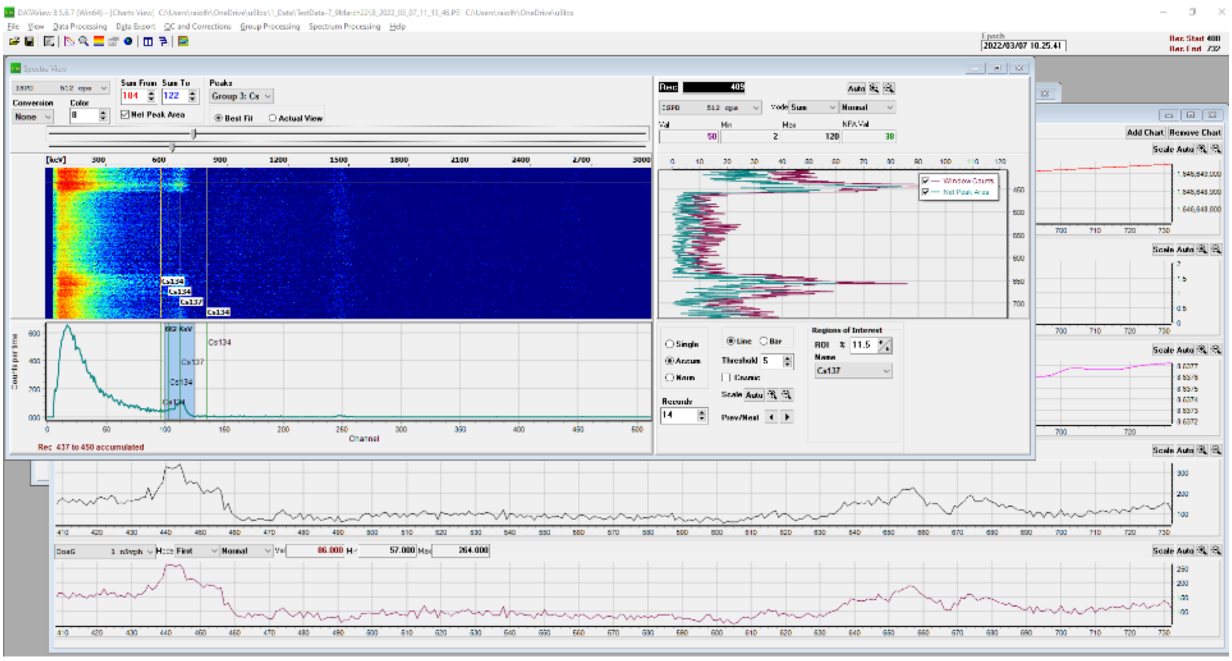

Figure 6: *Example of radiological data with the identified Cs-137 photo-peak (waterfall plot on the top left) (source DATAView software).*

The U-Blox binary data (see Data format) were collected and the analysis conducted was mainly based on the following messages:

- **UBX-NAV-PVT**: This message contains the Navigation Position Velocity and Time (PVT) solution with the position solution expressed in geographic coordinates. The solution recorded is the internal one computed in real-time by the receiver;
- **UBX-RXM-RAWX**: This message contains the multi-GNSS Raw measurement data, such as pseudo-ranges, Doppler frequencies and carrier phases. This message provides information for all GNSS and frequencies supported.

These messages encoded in a binary format, parsed and converted into text files with tabulated values before being able to perform additional processing. For the conversion, a data parser was developed (see Figure 7).

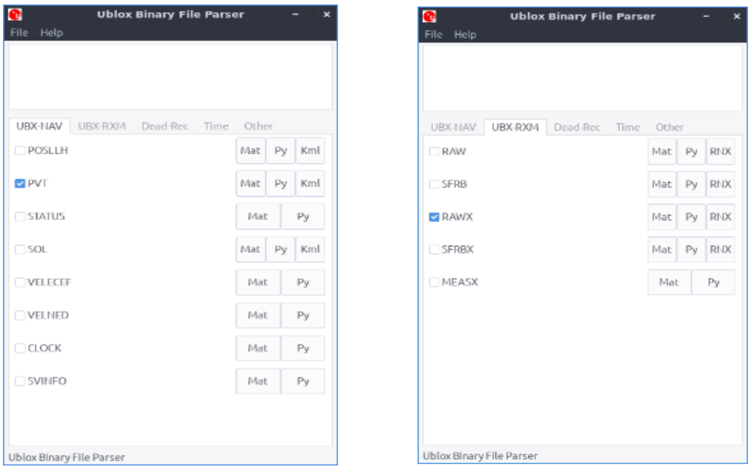

Figure 7: *Views of the U-Blox Binary File parser developed to convert the U-Blox binary messages into text files with tabulated values (source Parser application).*

It is important to remark that U-Blox receivers are highly configurable devices. The u-center software (see Figure 8), used for data logging and receiver configuration, provides a user-friendly interface allowing direct access to the different receiver options. U-blox receivers rely on a filter to improve the quality of the position solution. This filter uses a dynamic model that needs to be configured according to the specific conditions of the data collection. Several pre-configured filter settings are available and can be set from the U-center configuration panel. The "*Pedestrian*" dynamic model was selected for all the tests.

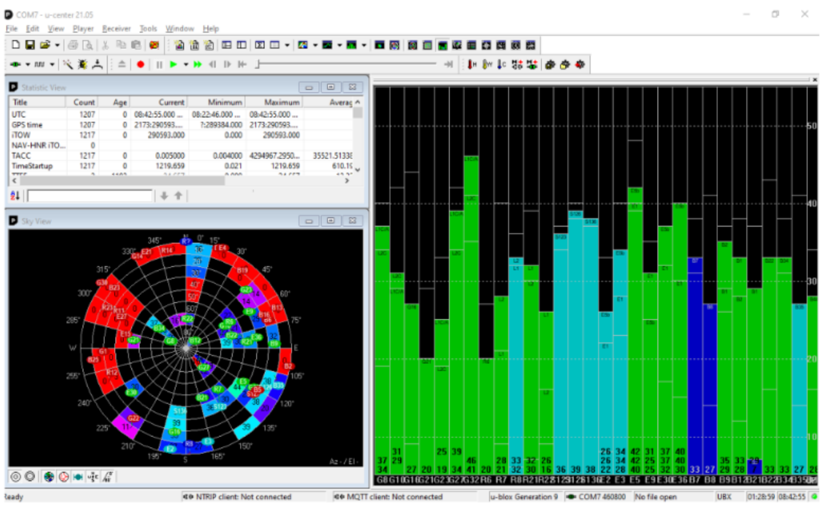

Figure 8: *U-center software for communicate with Ublox board (source U-Blox software).*

Pedestrian mode sets specific conditions on the registration of geo-localisation data that are necessary for further analysis.

When using Android smartphones, the GNSSLogger App was adopted for the data collection. The application is able to log several data types from the smartphone including PVT information and GNSS raw measurements.

Data are recorded in a text file containing different information in the specific we used the following messages:

- *Raw*: these messages contain raw GNSS observables (see developer.android.com for a detailed message format description). These messages have been converted into *RINEX* files
- *Fix*: these messages contain the position solutions computed by different providers.

Providers are different hardware/software sources (GNSSlogger, see 'About this App' section) tht provide position solution. In the tests conducted, only the GPS[4] and FLP[5] solutions were consistently available.

Python script was written to extract the "Fix" messages and convert them into tabulated text files organized in a way similar to the pvt files obtained from the U-Blox PVT binary messages. These files were also converted in Kml files. This generated text files are similar to those obtained for the U-Blox receivers.

It is evident the creation of a large number of different recorded data formats in the data collections because of heterogeneity of the devices used and for their ability to provide data according to different standards. Figure 9 summarizes the different data formats adopted and the conversion steps performed. As already discussed, for U-Blox receivers, the U-Blox (ubx) binary format was mainly used: from UBX-NAV-PVT messages, PVT information was extracted and converted into text files with extension *pvt*. These files contain tabulated values of the different position fixes. *kml* files were also generated and used for the plots obtained with the QGIS software. UBX-RXM-RAWX messages were also recorded and used for the generation of RINEX files.

When U-Blox binary messages were unavailable, NMEA messages were adopted for the generation of the pvt and kml files.

The GNSSLogger app was mainly used for Android smartphones. The fix data with two different providers (GPS and FLP) were used to generate ".pvt" and ".kml" files, and the raw measurements were used to generate RINEX files.

---

[4] Internal solution provided by the GNSS chipset integrated into the smartphone.

[5] Fused Location Provider, which combines information from the GPS and NLP solutions to provide improved PVT data

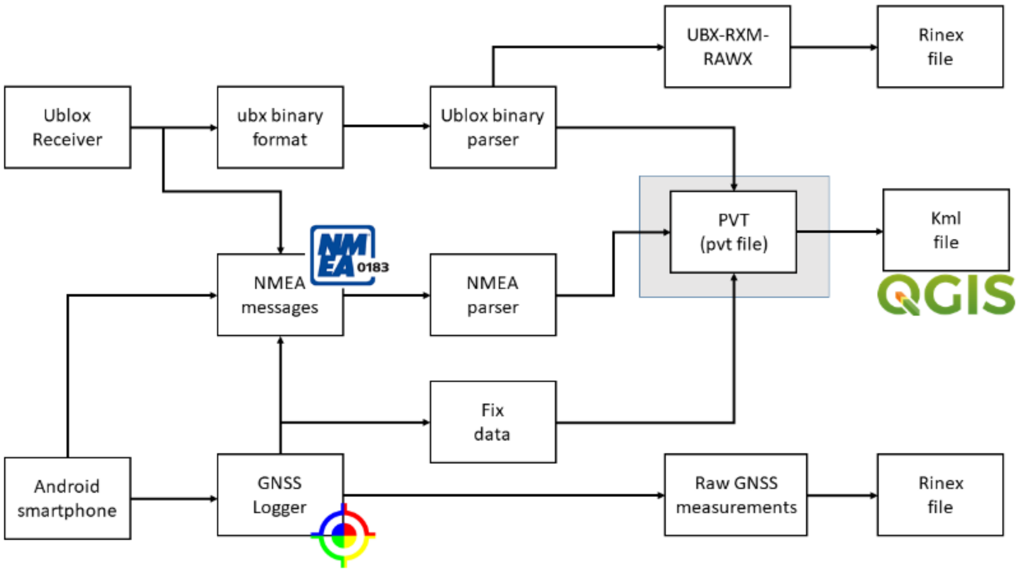

Figure 9: *Different data format and conversion options used during the data collections.*

In conclusion, PVT information from the different devices was converted into *pvt* text files with a common format. Having data organized in a common format allowed a simplified and direct comparison of the position solutions obtained.

The two days measurement campaign concluded with 26 radiological measurements acquired for dynamic geo-localization with 5 different GPS systems and a NuHLS-100 RIID radiological set of associated measurements in the outside Area 52.

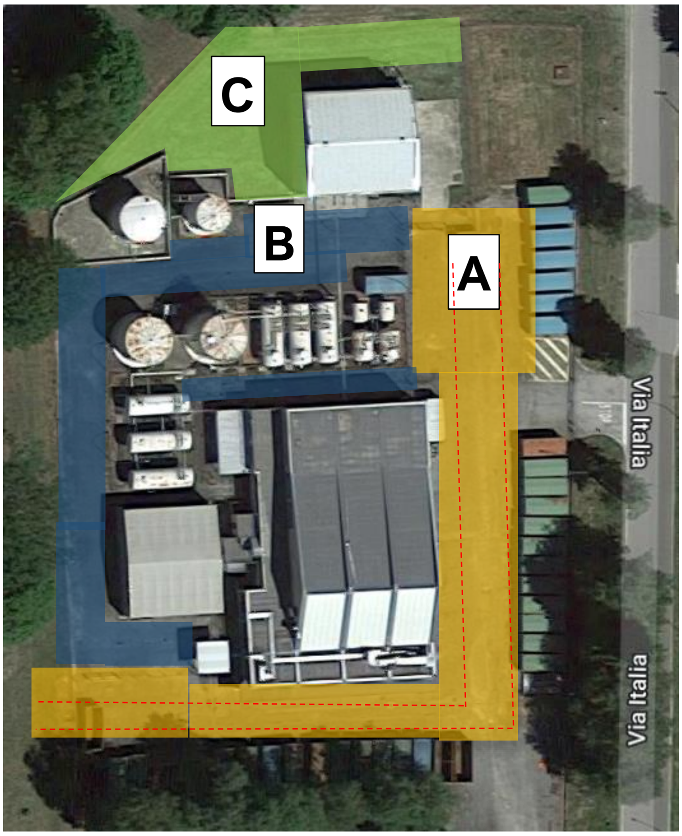

Figure 10: Radiological plan map for Area 52 (three zones of interest). The red dashed line identifies a measurement path (source Google Map).

On the same Area 52 a second radiological survey was performed on the October 2022 in a four-day operation with an Unmanned Aircraft system (UAS) from contractor. The UAS consisted of a UAV (aka drone or BRUS-H, H stands for heavy), a payload (DRONE-G) and a ground control system (see Table 1 and Figure 11).

Table 1: Characteristics of the BRUS-H system.

BRUS-H	BRUS-H payload
▪ Diameter 120 cm ▪ High 50 cm ▪ Propeller (ø) 30“ ▪ Number of propellers 6 ▪ Construction C-F composite ▪ Power unit BLDC electric motors, 6× ▪ Motors input (Total) 6×800 W ▪ MTOW 25 kg ▪ Maximal load capacity 10 kg ▪ Maximal speed 70 km/h ▪ Maximal endurance 90 min ▪ Standard endurance 50min (depending on load, wind and battery) ▪ Wind resistance <12 m/s ▪ Additional property Dust, snow and rain resistant system	▪ Plastic detection module 1 litre (200x100x50mm) ▪ sensitivity 500cps @ 100nGy /h ▪ energy range 50kV to 3MeV ▪ Maximum throughput 100kcps ▪ NAI3 Module with 3x3” NaI(Tl) ▪ NAI2 Module with 2x2” NaI(Tl) ▪ Resolution NAI3 <7.5% @ 662keV Cs-137 ▪ Resolution NAI2 < 7.0% @ 662keV Cs-137 ▪ dose rate 50nGy – 50µGy/h ▪ Maximum throughput 50kcps

▪ Temperature -20 °C to +50°C ▪ DRONES-G Base module: o Data transmission 868MHz o Video transmission 5.8GHz	▪ Spectroscopic data are transmitted to the Ground Station and simultaneously recorded on the Micro SD card

The BRUS-H (see Table 1) is a military grade unmanned aerial vehicle designed for environmental reconnaissance, rescue operation and operative monitoring of hazardous areas. It is loaded with a NuEM DRONES-G Module, a state-off-the-art technology for light airborne monitoring using drones as carriers. The system offers excellent performance for environmental radiation inspection and emergency monitoring.

The DRONES-G is a modular detection and gamma spectroscopy system independent from the carrier. It is self-containing, self-powering and rugged for field applications (see Figure 11 – right picture).

The following QR code will help to visualize the size of the BRUS-H in augmented reality enabling you to understand how and if to apply on your specific case.

	The QR code on the left will give you access to an AR visualisation of the UAV by using a phone or a tablet with a camera. It will help to visualize in a real environment the instrumentation (website 000webhostapp.com). Click on *Start AR KP WebXR* and tap on the phone screen to visualize it in your environment. Wait for loading the model.

An area of $\sim 8100\ m^2$ was scanned with two types of detectors: a plastic scintillator 1L and a NaI 3"x3" (see Table 7 and Figure 11 on the bottom); with different physical characteristics. In particular the plastic scintillator has good efficiency characteristics but has no spectroscopic capabilities (three energy regions could be post-processed for a general spectroscopic attribution) while the NaI detector have spectroscopic capability but lower efficiency.

In this campaign, the UAS registered:

- the dose rate in Gy/h,
- the counts pro sec (cps),
- the altitude by a LASER system, and
- the geo-localization of the drone.

The flight planners were constructed based on the area Figure 12 and of the buildings/structures/tanks present in the flight path ([2]-[4]). The full area was divided in four section: A, B, C and D (see Figure 12 and Figure 13); that permitted to optimize the flight time on the path and the altitude of the drone (i.e. the total flight time).

Figure 11: (Top) The UAS, the flight planner software and the radiological device DRONES-G NAI3 (source contractor). (Bottom) Plastic scintillator and the NaI 3x3" nuclear detector.

The flight path was optimised using specialized software (like UcGS, DroneArmony, DH Mobile and similar) to achieve the best flight time for the autonomy of the drone and to maximize the quality of the radiological data of the area. The area comprises many buildings and different type of structures (see Figure 12 b)) that required in many circumstances to use a full manual flight mode [12] [19] and [3].

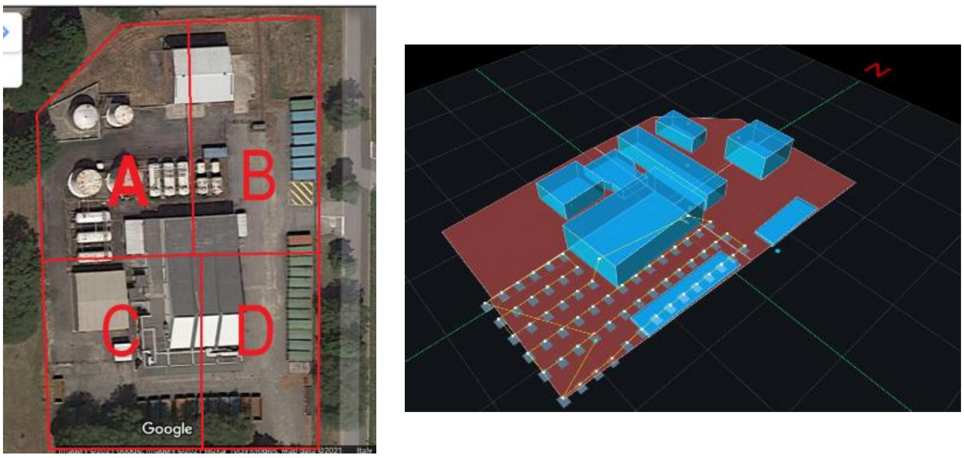

***Figure 12:** a) Preliminary flight planner with four sectors. b) 3D visualisation of the drone flight path in the Area 52 (source Google Map and DroneDeploy).*

The *SW DRONIC* provides the communication and data transmission between Base Module and Ground Station as well as acquired data visualization, status of connected modules, control over modules functionality and data recording on SD Card. The *SW DRONIC* application's main screen shows visualization of gamma spectrum with time history in the colour waterfall graph, below the real-time spectrum ($1\ sec$ or accumulated spectrum) as well as a time graph of a selected value from available values (altitude, dose rate, CPS and more) measured by the system and recorded on the SD Card.

Fourth radiological aerial flights of interest (or a set a multiple aerial scanning for flight) performed on area 52 that include different specificity are listed in the following graphical list[6]:

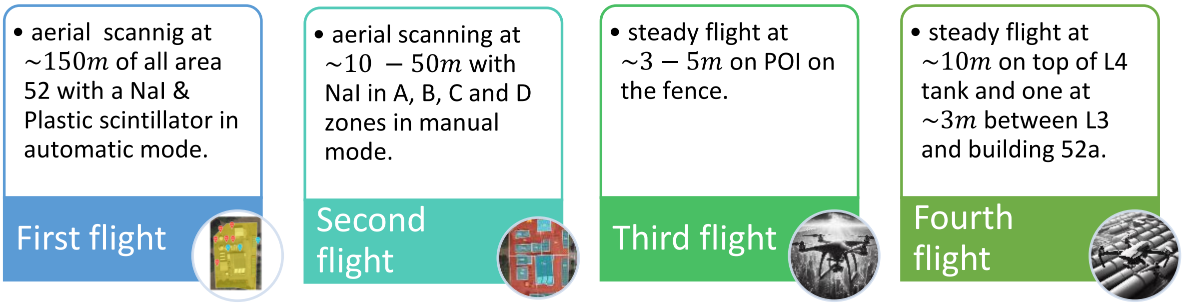

To examine the radiological data of some specific POIs (9 Point of Interest see Figure 13 A) that they have been envisioned during the previous radiological evaluation of the area (i.e. 2016 measurement campaign with a 25L Plastic scintillator [3]), we performed specific radiological surveys with the drone at a lower altitude ($\sim 3 - 5m$) to acquire spectrometry data and to possible identify some radionuclides in the area. We also registered the data on top of the highest tanks to have a general view of those regions (i.e. Area 52b and 52c, see [13]).

A	B

[6] The third and fourth images are generated with AI on 11 July'24.

C

Figure 13: *A) Map with the 6 POIs with easy UAV access (red) and three POIs with difficult UAV access (blue). B) Map of the four scanned sections with the relevant structures height. C) UAV flight path animation (source Google Map).*

At first, the drone radiological scanning was performed on the full extent of Area 52 (yellow shadow box and animation of the UAV flight path in Figure 13). The analysed radiological data are represented in the following figures as heat-maps with the 1L Plastic scintillator and the NaI 3x3“ (later on referred to as NaI_3) detector (see Figure 15). Those radiological maps were performed at $\sim 20m$ height and $3.5 km/h$ $(0.97 m/s)$. As it can be seen, both detectors registered a very similar radiological pattern in relation to the tanks T9, T10, T4, T5 and L4. The maximum registered value by the Plastic scintillator was $0.63 \mu Gy/h$ and for the NaI_3 $0.68 \mu Gy/h$. As for radionuclides composition, the NaI_3 identified only Cs-137 in the area.

Second, some extra zones extra zones were registered to cover all identified POIs (see Figure 13) of Area 52. Due to the specific structures’ restrictions surrounding those POIs, the drone was manually manoeuvred. The heat-maps (for the respective 5 POIs) were analysed and registered the CPS with both detectors. We also performed a flight on a spot (POI A2) just outside the fenced area, north of the entrance gate to Area 52, but we could not confirm the suspected hot spot identified by the past survey [3].

In the second flight, high CPS was recorded on top of the tank L4 and then in the region of the T3, T2, and T1 tanks (see Figure 14 for buildings/tanks distribution) followed by the relatively lower but still elevated CPS above T10, T9, T4 and T5. CPS value then returned to its maximum above T1, T2 and T3 remaining low when flying above tanks L1, L2, T8 and T9. The maximum dose rate appears to be emanating from the tank T1, although the highest dose rate had been expected on the T10 tank based on the values measured manually in the past measurements: up to $\sim 1\ mSv/h$.

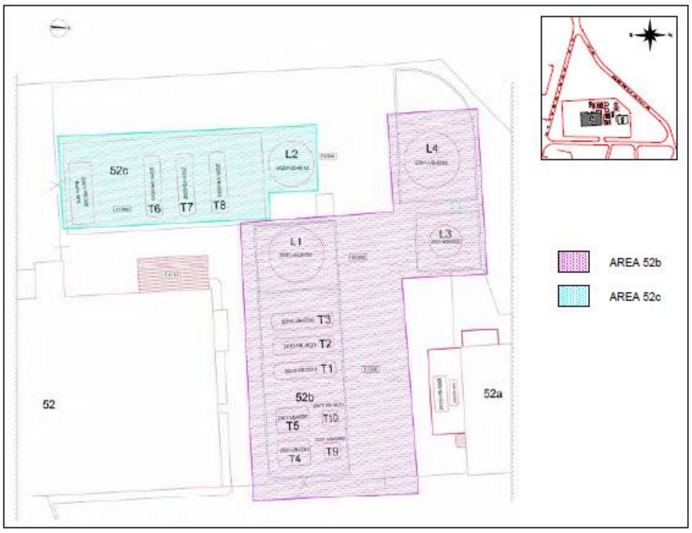

Figure 14: *Open air Area 52 General Layout.*

Plastic scintillator

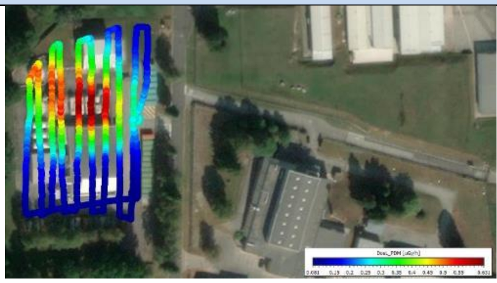

NaI 3x3”

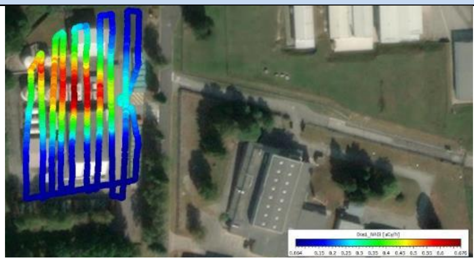

Figure 15: *On the top the heat-map from the Plastic scintillator. On the bottom the heat-map of the NaI3 detector.*

Those expectations were drawn from Table 19 in document [13], recapped below:

- The maximum value measured corresponds to Tank T10 (about $1\ mSv/h$) in a hot area located at its bottom.
- Tank T9 presents significant dose rates at some points although they are lower than Tank T10 values.
- Tanks T1, T2 and T5 dose rates are in the range of $50 - 200\ \mu Sv/h$.
- Tanks T4, L4, L1 and L3 dose rates are in the range of $15 - 50\ \mu Sv/h$.
- Measurements of remaining tanks (L2, T3, T6, T7 and T8) are below $10\ \mu Sv/h$.

The third flight was focused on the point of interest along the fence on the western side of Area 52. Also, this flight could not confirm the presence of the elevated CPS found during the land survey in 2016.

The final two flights are focused on the southwest corner between tank L4 and building 52a. Once again, the aerial measurement results could not corroborate previous detection of any elevated CPS in this area.

Overall, the aerial survey results indicate that soil in all outdoor areas of STRRL is not contaminated by gamma-emitting radionuclides beyond the natural background.

4.3. Regulatory & Licensing aspects

As the use of a portable radiological device (NuHLS-100) doesn't require special authorization in comparison to other similar tools for characterization in a decommissioning operation, it will be not considered in this document. While a specific authorization it is deemed for a UAS.

The use of drones (either purchased or designed and in-house constructed) for research or professional purposes within the JRC Ispra site can only be authorised by the JRC Ispra Site Manager[7] (JRC Directorate R – Support Services Site Management Ispra – Safety and Security) by filling the “request of authorisation.

EU Regulations 2019/947 [9] and 2019/945 (amended by Commission Delegated Regulation (EU) 2020/1058 of 27 April 2020 [2]) set out the framework for the safe operation of civil drones in the European skies. They adopt a risk-based approach and do not distinguish between leisure or commercial civil drone activities. These regulations consider the weight, specifications and the intended operation of the civil drone. EU Regulation 2019/947, which has been applicable in all EU Member States since 31 December 2020 (including Norway and Liechtenstein), addresses most types of civil drone operations and their levels of risk.

ENAC, the Italian Authority for Civil Aviation, implements EU regulations in Italy and legislates on the aspects that remain within the competence of the Member State. In fact, on 4 January 2021, ENAC published the UAS-IT Regulation [20] on the use of drones, applicable from 31 December 2020, to complete the legal framework of EU regulation 2019/947 for the aspects for which this regulation refers to national provisions.

Since 2015, ENAC has been cooperating with ENAV, the Italian Air Navigation Service provider, to establish the technical and operational conditions for the safe and secure use of drones in different operational scenarios.

For the UAS operation in the JRC-Ispra premise it was mandatory to submit a flight plan and complete the Specific Operation Risk Assessment evaluation (SORA) for open category A3 and UAV of $<26kg$ payload (see Figure 16).

> ⚠ We encounter few initially difficulty due to a first kind of UAV activity for the contractor with the specificity of this scanning but we received a great support by Site Management Ispra, to facilitate the administration.

[7] The JRC site is registered as “No-Fly-Zone” (for altitude < 2.000 feet = 609.6 meters) identified as “LI P 57” on the aeronautic maps issued by ENAV.

1.Hazards Identified and potential harm it could cause	2. People At Risk	3.Controls in Place	4.Risk Rating				5. Action
			L	S	Score	Risk	
Personal injury caused by loss of control of UAV (e.g. persons hit by falling UAV or by elements of the UAV (e.g. propellers).	S, C, V	The drone pilot has completed an appropriate course of training, is a licensed drone operator and has more than 100h of drone flight experience. The drone pilot will strictly follow the EU Regulations 2019/947 and 2019/945. The area of drone operations will be monitored and possibly fenced off to prevent access of uninvolved persons.	2	2	**4**	LOW	Monitor
Specific system-related injuries	S, C, V	All involved persons will receive from the drone operator instructions and safety precautions to be applied in case of an emergency situation. The drone hardware and software is maintained according to the manufacturer's instructions and in perfect working order. The operator of the drone must only operate the drone if he is reasonably satisfied that the operation can be completed safely.	2	2	**4**	LOW	Monitor
Conflict with manned aircraft	S, C, V, P	Conduct pre-flight survey of area to identify no-go/no-fly zones and reliable lines of sight	1	3	**3**	LOW	Monitor
Uncontrollable movement of the UAV	S, C, V	Continuous visual supervision with UAV and connection control and a close safe buffer zone	1	3	**3**	LOW	Monitor
The UAV falls due to low batteries	S, C, V	Setting a sufficient reserve of battery capacity before takeoff. Take-off cannot be performed without setting this parameter.	1	4	**4**	LOW	Monitor
Propelers damage	S,C, V	Visual precheck before take off and during hovering on Home point	2	4	**8**	LOW	Monitor, review & reduce risk where possible
Drone-G modules release and fall to ground	S,C,V	Visual precheck before take off, Plan the survey route out off people standing	3	4	**12**	MEDIUM	Monitor, review & reduce risk where possible

Figure 16: *On the left, the SORA evaluation on the 2 days flight plan in Open Category A3, On the right, the flight plan of the area and the emergency and start/stop position (red cross) (source Google Map).*

4.4. Quality aspects and data

The data acquired in an outside environment combines radiological and geo-localised data. The team performed a set of measurements that addressed the accuracy and repeatability of the data. The results are shown in chronological order and focus on the geo-localisation quality of the data in a dynamic mode. Additional measurements were also considered and their reasons are indicated.

This document presents the data in a table Table 2 showing their geo-localized position (figure on the left) and statistical data (table on the right). The technical documents leave the analysis details to the reader [16].

A preliminary **static** test (detection system in a fix position) was used to study the dispersion of the geo-localized position solutions determined by the U-blox F9P device and by the receiver integrated within the PGIS-2 instrument. The point selected for the data collection and denoted as A1 (see Figure 1) was also used for background observations and for studying the background condition of the radiometric measurements. A table (Table 2) will summarize the data in terms of their geo-localized position (map on the left) and the statistical data (table on the right). The detail of the analysis is left to the reader on the technical documents [16].

The scatter plots of the position solutions determined by both receivers are provided in the top figure in Table 2. These are heavily filtered in time. The operator performing the test confirmed though visual inspection of the corresponding orthophoto that the position solutions of the U-blox F9P device correspond to the actual device position. For this reason, the U-blox F9P position solutions are considered unbiased.

A static test for about 360 seconds (conducted under relatively mild propagation conditions) was used to study the dispersion of the position solutions determined by the U-blox F9P device and by the receiver integrated within the PGIS-2 instrument. The point selected for the data collection and denoted as A1 was also used for background

observations and for studying the background condition of the radiometric measurements. In this case, no smartphones were used for the test.

The standard deviation of the horizontal components of the F9P solutions is significantly lower than $1\ m$ and the main dispersion is observed along the North direction.

Then, a second step was to conduct a series of radiological measurement in a **dynamic** mode in six different sections and area of the region of study as specified in §1: sec.A, sec.B, Sec.B3, sec.C1, Area-40 and Area-52.

In relation to the dynamic test outside in Area 52 a set of data analysis has been performed and the following section will describe the analysis and results of them. The summary Table 2 will indicate with a plot (on the left) the GPS track and repeatability of the data, the standard deviation determination and the scope of those tests. The data, in general, reveal that android phones even if they show an improvement in comparison with PGIS-2 have still a very significant North and East std. deviation errors. Then they are not suitable for mapping radiometric measurements. This is mainly due to the difficult propagation conditions that make this type of environment too harsh for smartphone receivers. For this reason, this report won't provide those data (see for details [5]).

In the paragraphs below and following Table 2, we will describe and highlighted the characteristics of each measurement to provide the reader with important details to be considered.

In each tests of sec.A, the operator performed the trajectories estimated by the U-blox F9P receiver (green) and by the device integrated within the radiometric instruments (red). The operator confirmed that the trajectory estimated by the U-blox device corresponds the actual path followed during the test and that no major biases could be identified. On the contrary, the trajectory estimated by the GPS (Global Positioning System) device is irregular and exhibits patterns significantly different from that actually followed by the operator. It is noted that the trajectories estimated are in both cases heavily filtered. When the filter adopted is not properly initialized, significant biases occur and are propagated for the whole trajectory.

Table 2: *Plot of the position solutions determined by the U-blox F9P and PGIS-2 receivers for all performed test in dynamic and static.*

STATIC TEST

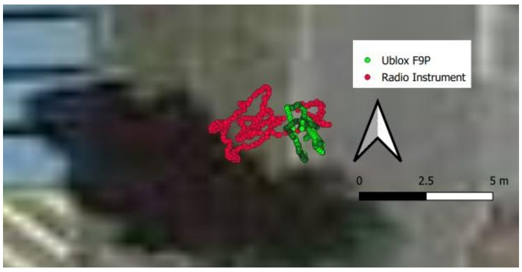

Pos. A1

	U-blox F9P	PGIS-2
East Standard Deviation (cm)	34	113
North Standard Deviation (cm)	71	84
Mean East offset wrt F9P (cm)	0	-179
Mean North offset wrt F9P (cm)	0	26

Scope

~6min static measurement to study the dispersion of the position solutions determined by the U-blox F9P device and by the receiver integrated within the PGIS-2 instrument.

DYNAMIC TEST

<table>
<tr><td>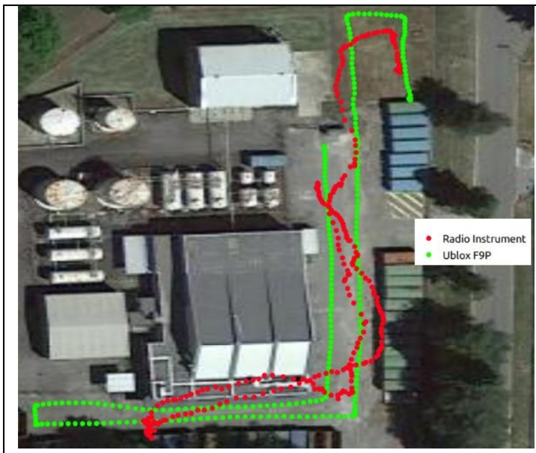
</td><td>Sec.A</td><td>Test 2
Test 3
Test 4</td></tr>
<tr><td rowspan="4">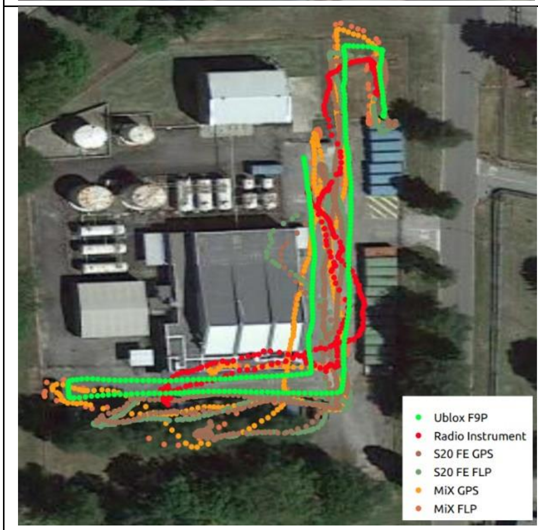
</td><td>Sec.A</td><td>Test 1</td></tr>
<tr><td></td><td>U-blox F9P</td></tr>
<tr><td>East Standard Deviation (m)</td><td>0.23</td></tr>
<tr><td>North Standard Deviation (m)</td><td>0.19</td></tr>
<tr><td colspan="3">Scope</td></tr>
<tr><td colspan="3">5 total test were the test2-4 used only the U-blox F9P and the GPS receiver integrated in the radiometric instruments. While in test 1 we used two additional devices, a Samsung S20 FE, and a Xiaomi MiX .</td></tr>
<tr><td rowspan="4">
</td><td>Close Loop</td><td>Four loops</td></tr>
<tr><td></td><td>U-blox F9P</td></tr>
<tr><td>East Standard Deviation (m)</td><td>0.13</td></tr>
<tr><td>North Standard Deviation (m)</td><td>0.19</td></tr>
<tr><td colspan="3">Scope</td></tr>
<tr><td colspan="3">A mild propagation scenario of $\sim 20m$ with four loops for repeatability and accuracy in East and North components. Accuracy of the different solutions of PGIS-2 and android phones using U-blox F9P as reference.</td></tr>
</table>

<table>
<tr><td rowspan="4">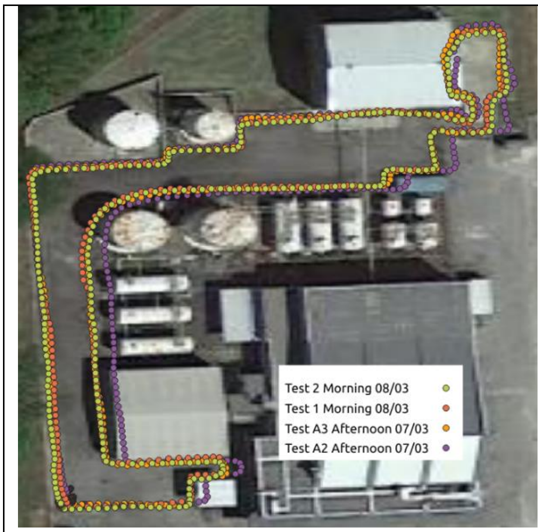
</td><td>Sec.B</td><td>Test A2
Test A3
Test 1
Test 2</td></tr>
<tr><td></td><td>U-blox F9P</td></tr>
<tr><td>East Standard Deviation (m)</td><td>0.39/0.14</td></tr>
<tr><td>North Standard Deviation (m)</td><td>0.14/0.13</td></tr>
<tr><td colspan="3">Scope</td></tr>
<tr><td colspan="3">Four trajectories recorded in Sec.B for accuracy of the different systems (PGIS-2 and android phones). Standard deviation with and without the test A2 (second values in table). Showing the trajectory of test A2 (purple track) clearly biased. In test A3 where android phones were used the PGIS-2 performed the worst.</td></tr>
<tr><td rowspan="4">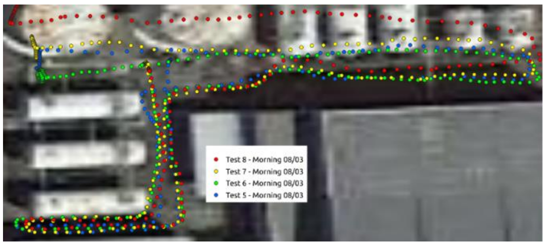
</td><td>Sec. B3</td><td>Test 5
Test 6
Test 7
Test 8</td></tr>
<tr><td></td><td>U-blox F9P</td></tr>
<tr><td>East Standard Deviation (m)</td><td>0.21/0.18</td></tr>
<tr><td>North Standard Deviation (m)</td><td>0.18/0.10</td></tr>
<tr><td colspan="3">Scope</td></tr>
<tr><td colspan="3">Four tests in a narrow space path surrounded by tanks and walls of nearby buildings. The initial position of the user in Test 8 is erroneously determined (top left corner of the figure). Thus, this bias is excluded, and new values are determined (second column values in table)</td></tr>
<tr><td rowspan="4">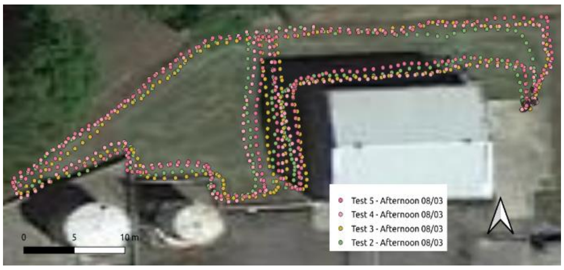
</td><td>Sec. C1</td><td>Test 2
Test 3
Test 4
Test 5</td></tr>
<tr><td></td><td>U-blox F9P</td></tr>
<tr><td>East Standard Deviation (m)</td><td>0.15</td></tr>
<tr><td>North Standard Deviation (m)</td><td>0.17</td></tr>
<tr><td colspan="3">Scope</td></tr>
<tr><td colspan="3">Four tests conducted in the Sec. C1 under open-sky conditions. Consistency with previous cases.</td></tr>
<tr><td></td><td>Area-40</td><td>Area 40 test</td></tr>
</table>

<table>
<tr><td rowspan="3">
</td><td></td><td>U-blox F9P</td></tr>
<tr><td>East Standard Deviation (m)</td><td>0.31</td></tr>
<tr><td>North Standard Deviation (m)</td><td>0.36</td></tr>
<tr><td colspan="3">Scope</td></tr>
<tr><td colspan="3">One single test under open-sky conditions in a parking lot of Area 40.</td></tr>
<tr><td rowspan="4">
</td><td>Outside area52</td><td>Outside 1</td></tr>
<tr><td></td><td>U-blox F9P</td></tr>
<tr><td>East Standard Deviation (m)</td><td>0.88</td></tr>
<tr><td>North Standard Deviation (m)</td><td>1.26</td></tr>
<tr><td rowspan="4">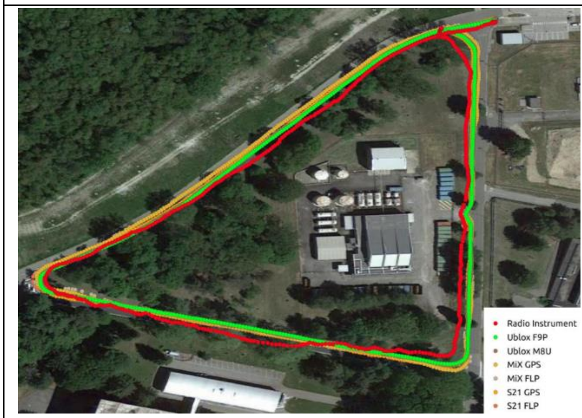
</td><td></td><td>Outside 2</td></tr>
<tr><td></td><td>U-blox F9P</td></tr>
<tr><td>East Standard Deviation (m)</td><td>0.88</td></tr>
<tr><td>North Standard Deviation (m)</td><td>1.26</td></tr>
<tr><td colspan="3">Scope</td></tr>
<tr><td colspan="3">Two tests were conducted outside Area 52. The first test performed by walking closely to the outside fence of Area 52 and the second in an even bigger area.</td></tr>
</table>

The solutions from the GPS and FLP providers were considered separately.

As for the previous case, the `U-blox F9P` is the only device able to provide a trajectory approximately corresponding to the path followed by the operator.

For this reason, the trajectory provided by the `F9P` device will be used in the following as reference. It is important to observe that repeatability analysis will be first conducted to assess the accuracy of the

F9P solutions and to justify the use of its trajectory as reference. Secondly the different solutions in different tests will be analysed for the F9P trajectory.

A set of tests (i.e. trajectories) in different sections of the Area 52 are performed to assess the followings:

- Repeatability Analysis – four trajectories
- Analysis Of The Trajectories Recorded Using Smartphones - four trajectories
- Close Loop Test

When analysing the quality of a trajectory provided by a GNSS device, a reference trajectory of better quality should be available (i.e. F9P trajectory). By comparing the reference and test trajectory, one can assess the precision (low dispersion/variance) and the accuracy (lack of bias) of the test solution. This can only be done Assuming that the reference trajectory is more accurate and precise than the test solution.

- **Precision**, defined as the standard deviation of the trajectory can be assessed through **repeatability analysis**.
- **Accuracy**, intended as lack of bias can be qualitative assess through the evaluation of the human operator who performed the trajectory. With the help of ortho-photos and maps, the human operator can identify portions of the trajectory affected by significant biases that do not correspond to the path followed.

In the tests conducted, the most accurate/precise solution is the one provided by the U-blox F9P receiver. While a more accurate/precise solution would be needed to assess its quality, other types of analysis can be performed to characterise this solution.

Repeatability analysis is conducted by performing the same trajectory several times. The operator is always asked to follow the same path to minimize the differences between the different runs (a reference line/markers or other means could be used to improve the operator accuracy). This is obtained for example, by constraining the path and passing close or above fixed reference points or landmarks. Even under such conditions, the user will introduce some variability, worsening the estimated precision. In addition to this, differences in speed will scale the different path components (North and East) differently when considered as a function of time. Moreover, it is also necessary to properly align the start and end of each trajectory.

For this reason, the different trajectories cannot be directly compared. The **DTW**[8] method was adopted to scale and align the different trajectories to allow the comparison. In this way, corresponding points were found in the other paths for each point in the trajectory used as a reference. For each point average and standard deviation were computed. Finally, the overall standard deviations related to the North and East components were computed.

Table 3: *Standard deviation of the East and North components of the trajectories (see also picture on the left) recorded during the tests in Sec. A using the U-blox F9P device (trajectories impose in Google Map).*

[8] Vaughan and Gabrys (2016) [21] proposed to use the **Dynamic Time Wrapping** (DTW) approach to match the different trajectories solving the scaling issue caused by the different speeds. The DTW also solves the initial alignment problem since this algorithm finds for each point in a reference trajectory the (time) index corresponding to the closest location in a test trajectory

Component	Standard Deviation (m)
East	0.23
North	0.19
Sec.A	Test 3 Test 2 Test 4 Test 1

Accuracy, anticipated as lack of biases, was evaluated only in a qualitative way based on the operator's judgment.

The four trajectories recorded by the U-blox F9P receiver for the tests conducted in Sec.A are shown in figure above. While an overall agreement is found, the trajectory depicted in green (corresponding to Test 2) has a slight bias of about $2.3\ m$ visible in the bottom left and right part of the figure and circled in white.

Applying the DTW to the four trajectories and using Test 3 as a reference trajectory, the estimated precision (standard deviation) of the U-blox F9P device is summarized in table on Table 3. The standard deviations observed are around $20\ cm$.

After characterising the precision of the U-blox F9P solutions, the accuracy of the trajectories recorded using the different smartphones is evaluated.

For the first three tests conducted in Sec.A, only the U-blox F9P device and the receiver integrated within the PGIS-2 instrument were used. For this reason, only the accuracy of the PGIS-2 integrated receiver was assessed with respect to the U-blox F9P device.

In the fourth test a Xiaomi MiX and a Samsung S20 FE device were also used. The accuracies of the different solutions are provided in [5] §5.2.2. The accuracy is expressed in terms of East and Nord components. For each component, the mean and maximum absolute error are provided along with the associated standard deviations. As expected, the receiver integrated within the PGIS-2 instruments provides the worst performance with maximum errors above $20\ m$.

The FLP and GPS solutions of the MiX and S20FE device provide some clear improvements with respect to the PGIS-2 integrated receiver. However, the errors observed as still very significant and are not suitable for mapping radiometric measurements. This is mainly due to the difficult propagation conditions that make this type of environment too harsh for smartphone receivers.

To further characterize the performance of the U-blox F9P receiver and of the other devices under test, a relatively mild propagation scenario, close loop, was selected. This scenario is illustrated in figure on Table 2, which also provides the trajectories recorded by the different devices.

The test was conducted in a small square field of $\sim 20\ m$ side. The field is enclosed in a fence and the operator was constrained to walk as close as possible to it repeating the same loop several times.

Four loops were performed: the green trajectory representing the internal solution of the U-blox F9P closely follows the perimeter of the fence whereas the paths obtained from the smartphones and the PGIS-2 integrated receiver a clearly biased.

As for the previous test, repeatability analysis was conducted on the U-blox F9P solution. The trajectory recorded was divided into four loops which were then scaled and aligned using the DTW approach with the corresponding average standard deviations. The estimated standard deviations are close to that obtained in the previous test with an improvement with respect to the East component. This improvement was expected given the milder propagation conditions characterizing this test.

Similarly, to the previous test, the solutions obtained with the different smartphones and the PGIS-2 internal receiver were analysed with respect to the U-blox F9P receiver whose trajectory was used as reference. Summary statistics obtained for this test are provided in [17] §5.3. The internal receiver of the PGIS-2 device performs poorly also under these mild conditions. For the MiX and S20FE maximum errors and standard deviations are practically halved with respect to the previous test, clearly showing the impact of the reception conditions.

The four trajectories recorded using the U-blox F9P receiver for the tests conducted in Sec. B are showing that three trajectories practically coincide, while the path recorded during Test A2 is clearly biased (purple trajectory).

Thus, when performing repeatability analysis, the trajectory from Test A2 has shown a bias after applying the DTW transform and consequently is not use as reference curve for the DTW.

Summary statistics for the repeatability analysis are provided in Table 2. Since the bias is mainly in the East direction, the main impact of this trajectory is along this component. When this trajectory is removed, a standard deviation of about $14cm$ is observed. These values are close to that observed in the close loop test described above.

In Test A3 of Sec. B, as example, (Figure 17) we provide a comparison of the trajectories recorded by the different devices (PGIS-2 and smartphones). As expected, the PGIS-2 device (red trajectory) provides the worst performance with estimated locations far from those provided by the U-blox F9P device. The trajectories provided by the smartphones are qualitatively better than those provided by the PGIS-2 device and for certain portions of the tests are close to trajectories determined by the U-blox F9P. The details of the data for the full list of mobile devices are available in [5].

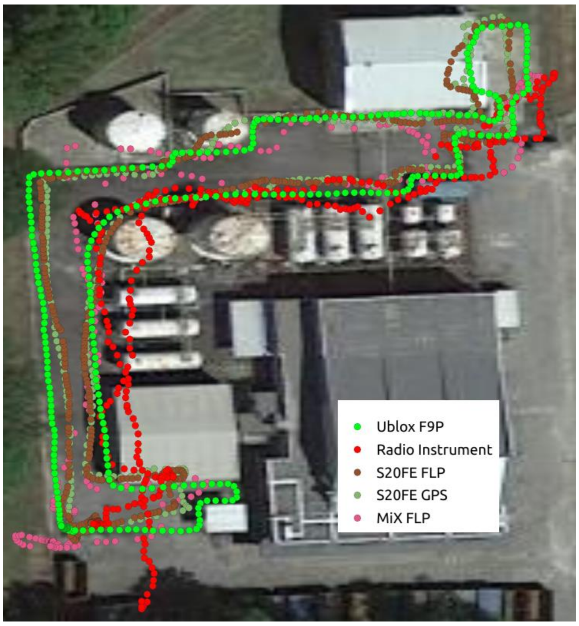

Figure 17: *Trajectories recorded by the different devices during Test A3 conducted in Sec. B.*

A set of tests was conducted in the Sec. B3 in a challenging testing area since the operator must move in narrow path surrounded by tanks and walls of nearby buildings. The trajectory obtained for Test 8 is clearly biased most of all in its upper part.

> U-blox F9P receiver implements a filter, based on the user dynamics, to propagate the user position. This clearly emerges from the much smoothed trajectories that are obtained. It improves the quality of the trajectory in terms of noise reduction but it can also propagate biases.

In Test 8 the initial user's position is erroneously determined (top left corner of the figure) and this bias propagated through the whole trajectory. This is avoided by the repeating measurement and by having a set of several trajectories, the biased ones can be excluded and the other can be used to compute median trajectories.

The four trajectories for Sec. B3 are further compared which provides the North and East components after applying the DTW transform. The associated standard deviations are provided with and without considering Test 8. The main bias introduced by Test 8 is along the North direction and this fact is clearly reflected by the standard deviations in Table 2. The details of the data for the full list of mobile devices are available in [5].

A set of tests was conducted in the Sec. C1 in a more benign environment since significant portions of the test have been conducted under open-sky conditions.

A good consistency between the different trajectories was observed after applying the DTW transform. The corresponding standard deviations are consistent with those observed for the previous cases. The details of the data for the full list of mobile devices are available in [5].

A single test was conducted in the parking lot of Area 40 – dynamic test under open-sky conditions. During the test, the operator followed a regular pattern aiming at covering the whole area of the parking lot and of the nearby road.

The two U-blox receivers used during the tests provide similar solutions with clear deviations and bias for the solutions obtained using the different smartphones. The accuracies of the different solutions in the table confirm the fact the solution provided by the U-blox M8U device is very close to that provided by the F9P receiver used as reference. Deviations are observable between the trajectories of the smartphones and of the U-blox F9P device.

Two tests were conducted outside Area 52. The first test was performed by walking closely to the outside fence of Area 52 and also, in this case the PGIS-2 is unable to provide an accurate solution.

The second test conducted outside Area 52 considered an even bigger area and performed by following the road around such area. As for the previous cases, the largest deviations are observed for the PGIS-2 device. The details of the data for the full list of mobile devices are available in [5].

Other additional tests have produced interesting results but for the scope of this document, I will only highlighted one of them from [5] that include an association between the GNSS and radiological data.

The test was conducted in Sec. B. It included the radiological data of PGIS-2 acquired during the track A2-A7 GNSS (Figure 18). Those values are expressed in CPS. The map is showing three regions of higher activity (i.e. $0.8, 2.1\ and\ 3.3\mu Sv/h$, respectively 1, 2 and 3 circles or a maximum value of $4647CPS$). Those three hot-spots are most likely not attributed to any ground contamination (see the extension of the path) but most likely to the vicinity of tanks/silos that contain traces of radioactive materials. A shielding lead around the sensitive crystal of the PGIS-2 should improve the position of the hot-spot/s in this type of environment.

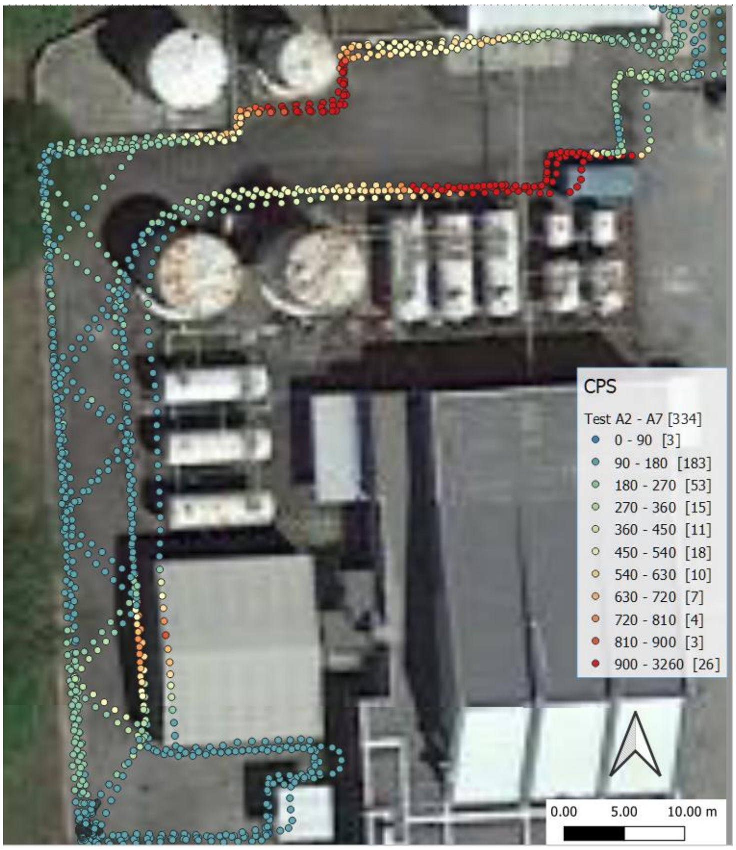

Figure 18: *Test in Sec.B with a CPS map.*

4.5. Findings and results

The previous sections demonstrated that the geo-localization with a GNSS system (like the U-blox C099-F9P) coupled with a radiological handheld device (NuHLS-100) could provide accurate radiological data and geo-localisation precision up to $\sim 20cm$ (i.e. F9P reference) if the reception conditions of GNSS signals are sufficient to guarantee proper receiver operations. The survey identified significant radiological activity in the STRRL area, primarily attributed to interference from external sources such as tanks and drums containing radioactive wastes (contained in). The presence of these sources made it difficult to accurately determine the ground's radiological levels. Further investigation is recommended to better understand the radiological status of the ground.

The current system is not an out off-shelf equipment; thus, it requires presence of a dedicated expert on the manipulation of the GNSS and radiological data. The radiological data needs to be extracted in a convenient format for the further analysis and integration with the GNSS data. The two time-series need to be synchronized, using the GNSS time stamps, and radiological data need to be properly associated to the corresponding location information. The time required for a fully validated result could be estimated for a single radiological track by the following experimental time, T_e, in days over metre (where *path* is the length of the track):

$$T_e\left[\frac{d}{m}\right] = \frac{(Rad+GNSS+Process+Python)}{path} \times N + \frac{T_c}{path},$$

where *Rad* refers to the extraction of the radiological data after their validation on a gamma spectra software, *GNSS* refers to the extraction of the GNSS data, *Process* refers to the conversion of the *ubx* file, *Python* refers to the analysis and the routine to combine the *Rad* and *GNSS* data, *N* refers to the number of possible iterations of the process for statistical error determination and a T_c, that it takes in account the combining of the different tracks.

> In the formula is assumed that the GNSS receiver is operating in real time providing its internal solution computed using an SPP approach.

The GNSS contribution for the experimental time, T_e, is equivalent to the processing time required to parse the data and extract the locations of the points forming the track. Raw measurements can also be adopted, and position solutions can be computed in post-processing using, for instance, corrections provided by international bodies such as the International GNSS Service (IGS). In this case, up to two weeks may be required to obtained precise orbit and clock corrections. While this option has not been evaluated in the current study, it would imply a GNSS time contribution of more than 2 weeks. In the following, only the case of real-time GNSS solutions is considered.

In the specific, for the Test1 ($\sim 50m$): $Rad = 1h \times photopeak$, $GNSS = 1h$, $Process = 30min$ and $Python = 1h$ and $T_c = 30min$. Then a value of $T_e\left[\frac{d}{m}\right] = \frac{18h}{50m} = \frac{0.36h}{m} \cong \frac{23min}{m}$ for four iterations and 2 photopeaks. The T_e is a roughly estimation of the processing and evaluation of the data but it doesn't include the operation time on field, the preparation of the instrumentation or the CAD drawings, neither the preparation and compilation of the scripts in *Python* or any other coding work to extract the information from the *ubx* or *PEI* files.

The use of a similar system GNSS+Radiological data will provide the following advantages that could be extended to different areas of the JRC-ISPRA site and more generally to other nuclear sites under decommissioning:

- Fast radiological survey of an area ($\sim 30m^2/min$)[9] with geo-localized dose rate and CPS data;
- Low cost of equipment;
- Wide applicability in outdoor area;
- Precise timestamp determination and possibility of data post-processing;
- Easy management of the software and extraction of the data.

Admittedly, the GNSS+RIID survey technique has also some limitations:

- Limited GNSS signal availability in tight spaces or significant obstruction of GNSS signal view;
- Need of a preliminary assessment of the GPS signal in the area;
- Availability of radioactive sources as reference points for accurate geo-localization and verified radiological base line;
- Long post-processing due to a not integrate system between the GNSS and the RIID;
- Precise radiological position of the NuHLS-100 (Pb shielding around the NuHLS-100).

[9] For a dynamic measurement at $0.75m/sec$ and a device solid angel of $\sim 1m^2$.

One of the improvement that is already in the modelling phase, will be the use of a lead shielding blanket around the PGIS-2 (see **Figure 5**). This shielding should improve the determination of the radiological hot-spot/s localization where interference from external radioactive sources could affect the results. Let's give an estimation of the area that the PGIS-2 can "see". We consider a NaI crystal of 3x3" and we assume that we kept a constant distance from the floor at about $12cm$. At the detector base (cylindrical crystal of $r = 2{,}54cm$ with a perfect lead collimator around the detector), the PGIS-2 will cover an area $A_{min} = 20{,}3cm^2$, while at the floor will cover $A_{max} = 95{,}9cm^2$.

Then the radiological scanned area will increase of ~ 4.5 times and therefore constituting a **limiting factor** for a precise localization as it can be visible on the standard deviation of the Ublox system (see Table 4). On this value we should also add the dynamic measurement, for which in one acquisition time ($1sec$) with PGIS-2 we span $\sim 75cm$ path length.

In the following table we can compare the results in term of cost effective and standard deviation characteristics of all the used systems. For this table we will use the average standard deviation from East and North data from the test in Area 40 and the one from close loop test (see [5] and [6]). Those two set of data represent the best open sky condition for GNSS acquisition. The time evaluation T_e is independent of the used system, while the precision could be one of the critical factors. Of course, we are comparing also four smartphone systems for which the primary target is not the GPS precision.

Table 4: *Cost effective use of geo-localized radiological system.*

Item	Device Cost [euro][10]	Time evaluation	Standard deviation [m] average bias
Reference standard procedure	1300,00	2d	NA
F9P + Antenna ANN-MB	287,00[11]	T_e	0.20
NuHLS100 + Fastrax UP501	100,00[12]	T_e	2.55
M8U + antenna ANN-MB	250,00	T_e	0.34
Xiaomi MiX	217,00	T_e	1.02
Xiaomi Mi8	530,00	T_e	NA
Samsung S20 FE	500,00	T_e	1.69
Samsung S21 Ultra	900,00	T_e	1.14
BRUS-H	7.500,00	18min	NA

As already observed the three smartphones are not suitable for a precise GPS localization and they should not be considered as the benchmark comparison. On the other side the F9P and M8U are the real term of reference devices against the PGIS-2 RIID (Fastrax UP501 antenna) for which it is possible to relay on the internal GPS ANN-MB series, L1/L2 multi-band. It is worth mentioning that is possible to use an external GNSS system of better quality or even use our U-blox system in PGIS-2. In summary, the two U-blox system can reach a fraction of a meter precision while the rest is over a meter.

[10] Smartphone costs are very variable due to different phone-package by mobile company. Those are average retail costs. The BRUS-H cost refer to a 3d rental price for the survey, radiometric engineer and UAV pilot.

[11] Unit cost of the product at the time of the invoice.

[12] This is a roughly cost pro-day to rent the RIID.

The aerial radiological survey using drones can be taken as a fast and reliable general and qualitative radiological survey of a large area, where through the use of innovative digital technologies including different nuclear detection systems on a drone, it is possible to create a comprehensive radiological heat-map of a relatively large area in a short time ($\sim 18min$). Of course, the data has to be corroborated by a deep analysis, where the current UAV cannot easily access, through for example the use of a hand-held spectroscopic device like the NuHLS-100.

The use of an UAS will provide the following advantage that could be extended to different areas of the JRC-ISPRA site (e.g. Area 40) and more generally other nuclear sites under decommissioning:

- Fast radiological survey of an area ($\sim 450m2/min$) with dose rate and CPS data.
- High resolution and geo-locate radiological heat-maps;
- Great efficiency and spectrometric capability;
- Reliable flight repetition through a flight planner software;
- Facility to exchange type of detector for different analysis purpose and multi-detectors payload;
- Flexibility of different altitude to compensate the distance-efficiency of the detector;
- Long flight time (in specific environment condition up to $\sim 45min$)

Admittedly, the aerial survey technique has also some limitations:

- Low manoeuvrability in tight spaces;
- No possibility of shielding detector;
- High altitude for safety condition.

This work was implemented by the operational team of CONTRACTOR composed of:

- Project Manager of the Contaminated Soil Management – Vladan Stefula (CONTRACTOR)
- APR pilot – Radek Nezval (CONTRACTOR)
- Payload operator – Tomas Grisa (CONTRACTOR)
- Operational and scientific support in Area 52 – Francesco Raiola (CONTRACTOR)
- Ispra Site Manager – Stephan Bonnet (CONTRACTOR)

4.6. Potential Benefits for Other Organizations

The application of this case study could produce the following benefits:

- Time efficiency: with a set work procedure and an optimisation of the path under characterisation.
- Cost workdays: reducing the man-days as in term of time and number of workers.
- Replacement of contaminated components: lower cost of these or similar UAS due to the increasing demand on the market (i.e agriculture, inspection, construction industry) as foreseen an increase for example in construction industry from $4.8bn to $6.2bn (source Drone Industry Insight).
- Regulation in place: as most European countries have implemented on their national aviation system the UAV rules, there a smoother and easier process for certification and authorization. Lower the cost of administrative tasks.

The use of those technologies in an outside environment by a semiautomatic and automatic process can support the facility characterization. Thus, as the market as shown and this case study had analysed the possibilities could be extended to other organization in the same sector (as other sectors already demonstrated their utilization) if a specialized team of nuclear operators are inserted in the organigram.

5. CASE STUDY No.2

5.1. Case Study Description

At the JRC-ISPRA in the STRRL [2], in the frame of the specific contract SC59 and as Part §4 of it - *Geolocation and Mapping* - a technical team performed two days of radiological geo-localized measurements inside buildings 52 and 52a. We used two system: a GNSS U-Blox C099-F9P-1-03 receiver, the NuHLS-100 contractor Instruments, a nuclear NaI portable detector for a set of dynamic radiological measurements inside the two areas and a LiDAR MLSP, a 3D portable system for the position determination inside the two buildings.

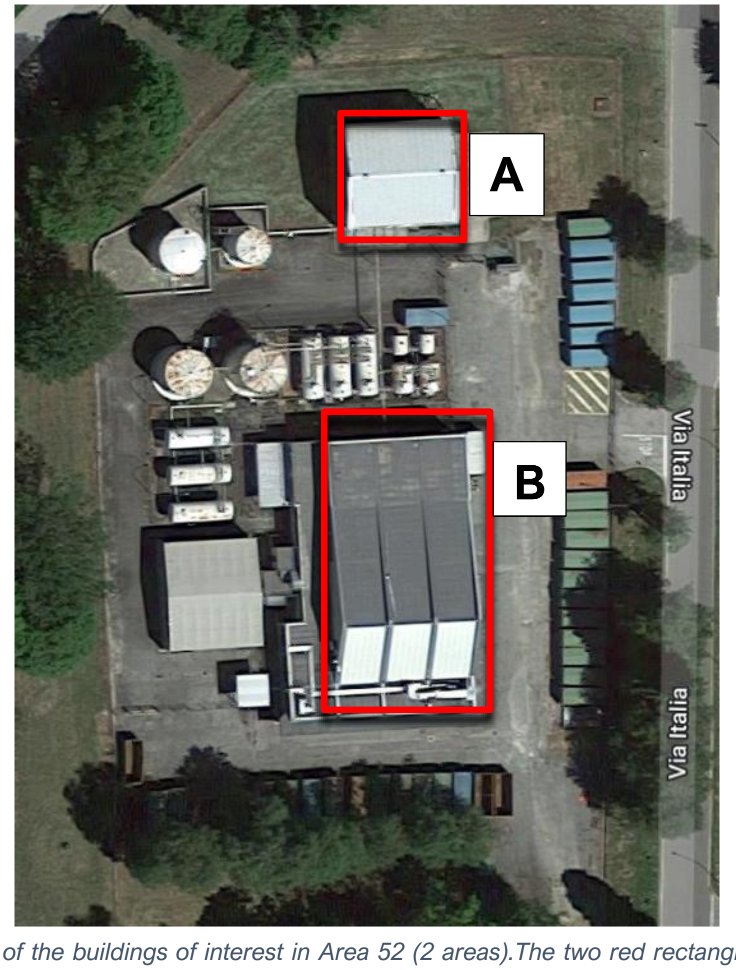

Figure 19: *Overview of the buildings of interest in Area 52 (2 areas).The two red rectangles represent the two buildings under survey (A. bldg.52a and B. bldg.52).*

The Area 52 in STRRL (see Figure 19) has two main buildings (encircled in red) named 52a and 52, see A and in B boxes respectively in the picture. For both, as planned in the work procedure [3], we considered two simple walking paths to cover as much as possible the internal area and for which a trolley was used to carry all instrumentations (see Figure 20).

Completed setup for the in-field measurements

Velodyne LiDAR scanner (grey cylinder) and ANN-MB antenna for GNSS (flat black patch)

Tablet for the acquisition of the data and the visualisation of the preliminary map

Figure 20: *Overview of the used instrumentation for the geo-localized radiological survey inside the buildings in Area 52.*

Thus, on March 2022, geo-localized radiological measurements were undertaken in STRRL in accordance with the plan [4]. The main objective of these measurements was to identify the state of the art and innovative technologies for geolocation of radioactivity measurements and to test them in full-scale project conditions on inside building. This work is connected to the Case study No.1 §4.

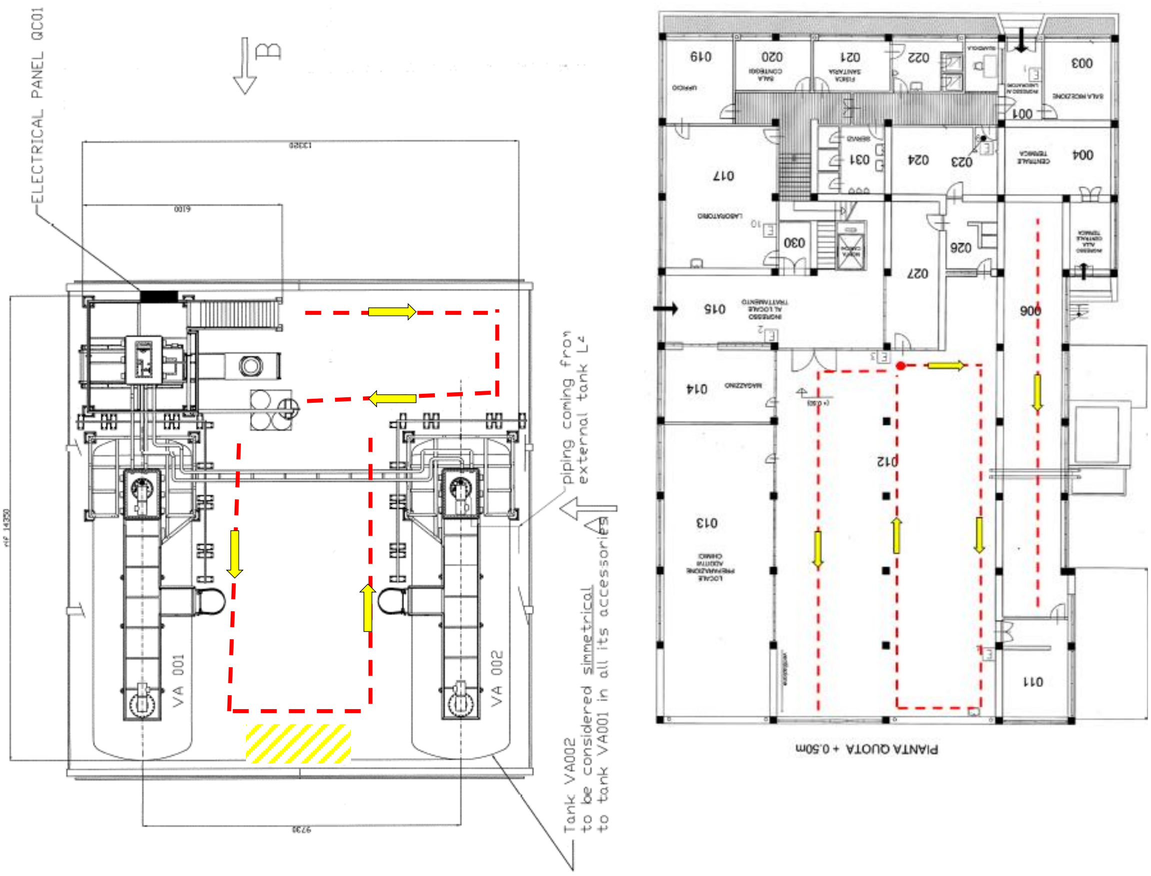

Figure 21: *Paths for two radiological survey in Bldg. 52a (on the left) and in Bldg. 52 (on the right). Yellow box represents an area with a highly radioactive materials in a containment box.*

To perform this field measurement the team used the following instrumentations for radiometric and geo-localization recorded data of Case study No.1 §4.1 (see **Figure 3**) here re-cited for clarity:

1. NuHLS-100 (aka PGIS-2 or RIID[13]) nuclear detector with NaI(Tl) crystal (0.347 litres) and android phone S5;
2. MLSP LiDAR and post-processing tablet;
3. UBlox C099-F9P-1-03 development kit equipped with a ZED F9P receiver with dual-frequency capabilities (aka U-blox).

The new device used in this case study is the Mobile Laser Scanning Platform (MLSP), a portable system that relies on LiDAR (class 1) and inertial sensors to perform two main tasks mapping and tracking in both, indoor and outdoor environments. This wearable system takes 600.000 points per second with a max survey accuracy of $\sim 2cm$ producing a real-time 3D point cloud visualization. The LiDAR could work in continuous acquisition for $\sim 5h$.

MLSP and its companion processing software STeAM Desktop were developed by JRC.DDG1.G.II.7 - Digital Systems for Safeguards and Non-Proliferation initially for Nuclear Safeguards applications [22]. It is commercially available for other application domains through license agreement with Gexcel Srl (see [23]). In the context of a joint project, G.II.7 adapted the

[13] Radioisotope Identifier Device

technology (both in terms of hardware setup and processing software) to the needs of the radiological characterization.

MLSP can work in two modes: *mapping* and *tracking*. When working in mapping mode, the system estimates simultaneously the motion of the user and the map of the environment using SLAM (Simultaneous Localization and Mapping) algorithms. The output of the mapping process is a globally consistent 3D point cloud of the area visited (i.e., the reference map) [24].
Once a map is available the system can be configured to work in tracking mode. When working in tracking mode, the system estimates at 12Hz the pose of the user within the reference map with centimetre accuracy. Results (i.e., the 3D poses of the system as the user moves) are timestamped and reported in real-time. They are also stored in the system's internal memory together with all the sensors data for further post-processing, if required [5].
Operating the MLSP does not require a specific type of motion: it can be carried in a backpack by an operator or mounted into any kind of ground vehicle. If the system is rigidly attached to another sensor (e.g., a gamma spectrometer), it can be configured to report the 3D poses of the target device when working in tracking mode. This way, if the external sensor is time-calibrated with respect to the MLSP and their relative (fixed) position is known, the MLSP can be considered as a "high accuracy GPS" that geo-references the measurements of the external device in real-time.

At the beginning, for informative purpose, we registered also the geo-localized data by U-Blox C099-F9P-1-03 development kit (same device for outside geo-localized measurements in [4]). It comes with an ANN-MB multi-band, high precision GNSS antenna (see Figure 20). This antenna has a low form factor and can be easily mounted on the top of a stick to improve visibility conditions. Later on in this document, the presence of the ublox system will be disregarded because in an inside geo-localisation mode, its use is very limited. It was mainly utilized to test the number of satellites that it was able to acquire in this constrain situation to assess its limitation. Therefore, since the *u-center* evaluated less than 10 satellites, it was obvious to disregard the quality of this type of geo-localisation (see more on the specific document [4] for outside measurements). The u-center evaluation software provides a powerful platform for evaluation of U-blox GNSS receivers. With u-center, the data can be logged as well as visualized in real-time.

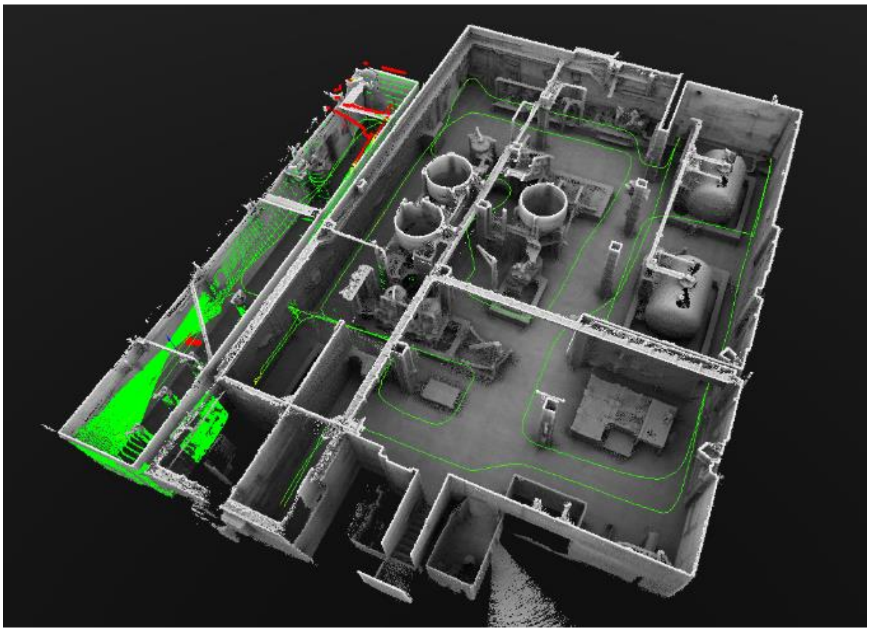

Figure 22: A reference map created by the MLSP in mapping mode (gray point cloud) together with the trajectory of the sensor estimated in tracking mode (green line). The live 3D data acquired by the LiDAR sensor is displayed in real-time as the user moves inside the environment (red-green coloured points), together with its estimated pose.

To carry all the instrumentation, a trolley (see first picture in **Figure 20**) has been chosen and external support has been designed by SketchUp Pro 2022 to adapt the NuHLS-100, a laptop, a tablet, ublox, and the MLSP system, as described in details in [4]. The locations of the different devices were carefully selected to optimize LiDAR scanning. This was done considering the space constraints of the trolley. A vertical stick was welded to the trolley and used to support the GNSS antenna and the LiDAR. In this way, the antenna and the LiDAR were placed at a relatively high position improving signal and optical visibility (clear view from the operator). The PGIS-2 instrument was kept close to the terrain and far from the metallic trolley structure to improve efficiency.

Besides, as in Case study No.1, it is important to reiterate that the effective PGIS-2 solid angle is rather large due to the absence of a collimator in front of the crystal. Thus, it will be influenced by radiation background around it. In the future, the idea is to use a lead blanket by standard lead bricks around the sensitive crystal to improve the precision of hot-spot/s position/s [4].

In the same context of a semi-automatic system in inside building this document describes the execution of a series of radiological measurements at the (LCSR) facility (114041_SC64_NT 04: THIRD SERIES OF NuVISION GAMMA CAMERA RADIOLOGICAL MEASUREMENTS AT LCSR [1], NE.45.2240.A.002: Concluding the INE, LCSR & Cyclotron plant characterisation [4]), to analyse the 15 hot-cells through the use of a NuVISION Gamma Camera device from NUVIA INSTRUMENTS. The entire campaign so far consisted of two sets of radiological measurements of the LCSR facility during the year 2021 for a total of 28.5 working days.

NuVISION is a portable spectrometric gamma camera[14] based on a 9,6cm^3 Cadmium Zinc Telluride (CZT) semiconductor detector with Compton imaging capabilities plus a coded tungsten mask *User manual NuVSION Gamma Camera*, Revision 2020/05 E, subject to technical changes [5]. The spectrometric capacity of the camera covers a wide energy range from 20 keV to 1400 keV (i.e., energy peaks from Am-241 to Co-60).

5.2. Quality aspects and data

The extraction and analysis of data from PGIS-2 utilise the following software:

The radiological data acquired from PGIS-2 (see RADaqLite manual [18]) are extracted by the PEIView software and converted in CSV format and used for the coupling with the GPS data.

The data from the PGIS-2 extracted in a CSV/TXT format (i.e. radiological data) are associated with the geo-localized data from the associated MLSP files using the column *SystemTime_sec* as common column.

---

[14] A Gamma-ray imaging consist of spatial mapping of gamma emitting radionuclides overlaid on a visual image of the scene.

Building 52a – tank farm　　　　Building 52

Figure 23: *Analysis of the different tracks taken with MLSP+PGIS-2 for the inside bldgs. 52a and 52.*

Briefly, the GI (see details in the Technical report NE.114041_SC64_NT 02Rev0: NuVISION gamma camera measurements at LCSR and Sec.6.1. therein) of NUVIA Instruments is a portable gamma spectrometric imaging[15] system for the localization, visualization and identification of ambient dose rate equivalent (H*(10)) on hotspots. The NuVISION gamma camera record a gamma radiation image superimposed on an optical image indicating the intensity of a gamma radiation and the nuclide type. In addition, the distance from the camera to the measurement points is measured by a LASER. Thus, the approximate dose rate of the radiation source can be estimated (i.e. at the head of the GI).

The gamma camera is mounted on a tripod for height adjustment and also on a swivel system to enable changing the FOV ($45°$ FOV of the device) when required. Through the NuVISION software, it is possible to perform a preliminary analysis during the measurement of the acquired information like: radioisotope identification and localisation, acquisition time, CPS, gamma spectra, distance determination (by laser method) for dose rate estimation, colour-coded hot-spots superimposed on the optical image, spectrum residual[16], dead time, etc. At the end of the measurements a final report is automatically created by the software with all the information that are reported in this document. The gamma camera is almost 4π shielded with lead sheet to reduce the incoming gamma radiation from different angles except the front and the back side of the GI (i.e. the CZT).

[15] A Gamma-ray imaging consist of spatial mapping of gamma emitting radionuclides overlaid on a visual image of the scene.

[16] This value expressed as a percentage represents the difference between the measured (and displayed) gamma spectrum (similar to χ^2) and the gamma spectra reconstructed after the detection of each isotope or line (peak) constituting the gamma spectrum.

To detect high energy sources such as Cs-137 or Co-60 that are out of the field of view of the coded mask aperture, we used 'Compton' option to visualize the Compton reconstruction of the current measurement (Compton camera imaging is a method to image gamma ray sources by measuring a Compton scatter and a photoelectric absorption for each decay in terms of positions and deposited energies). A location at the outer ring (a dashed red perimeter is showed during the measurement to indicate the current front FOV of the GI) corresponds to a source behind the NuVISION.

The background has an important impact on the accuracy of the measurements as it was observed in the previous campaigns [3], [6] [4]. As it is visible on the sketch of the area (see [4]-A) the hot-cells cover the entire area, the position and shielding of the gamma camera is important for the accuracy of the radiological results. Also [4]-B, –C and [4]–A to -D show the NuVSION GI in different position of the hallway during the full measurement campaign.

In agreement with the deductions from the first and second measurements campaign, the average dose rate (Avg. DR) acquired by the Area Radiation Monitor on the wall (two Else Saturn 5700/RTM instruments coupled with Geiger counters) was registered every day at the beginning of the measurements. These two sensors should cover the entire hallway and they recorded during the measurement week an average dose rate, $Avg.DR = 145{,}3 \div 231{,}7\, nSv * h^{-1}$.

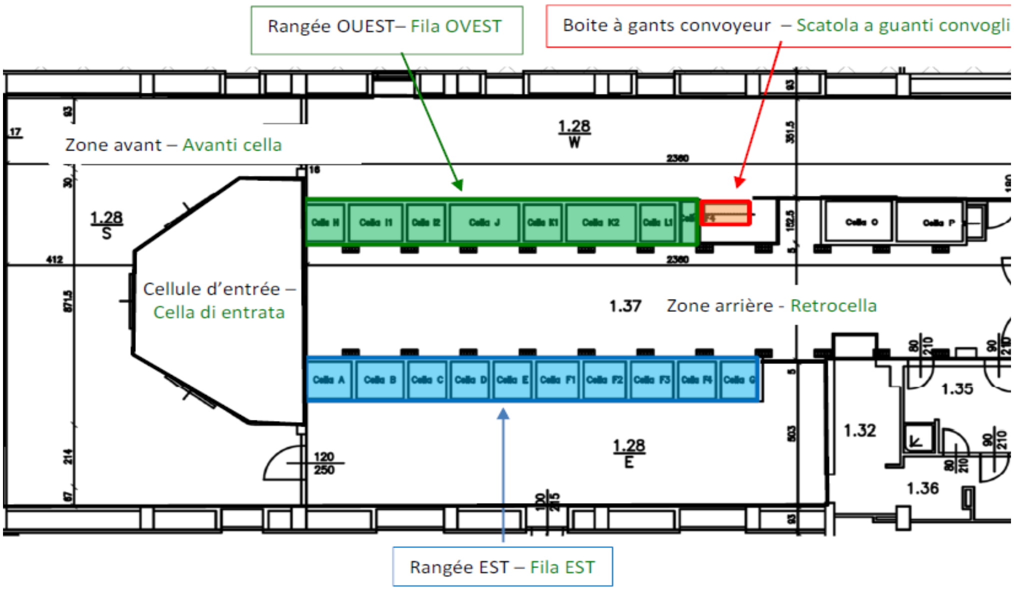

A. Hot-cells area with the two lines (EST and OVEST wings)

B. GI in front of a large type hot-cell (J)

C. GI in front of a large type hot-cell (K2)

A. Background measurement in front of the hot-cell G (the hot-cell was closed with the lead door)

B. Background measurement inside a lead shileding box

C. Background measurement in front of hot-cell F4-F3

D. Example of a measurement wihtout the Plexiglas (hot-cell G)

The information about the background condition in the area from the first and second campaign allow to understand better the background in the area.

However, we confirmed a high interference in the Cs-137 energy region during the background measurement in front of hot-cell D (on the back hot-cell J) with a $\text{Total dose rate} = 198{,}3\, nSv * h^{-1}$ and identification of the Cs-137 gamma line [4]. The camera identifies several hotspots and probably those are also from the camera backside (e.g., indication from the Compton analysis on the border of the image) with a $LT = 14139{,}3\, s$.

In the previous report, a background measurement was performed in a shielding box available in the area that covered completely the gamma camera on all 4π (see [4]-B). The analysed gamma spectra showed a $\text{Total dose rate} = 0{,}06\ [nSv * h^{-1}]$ with no evident radioisotopes identification. It is evident that the background conditions are extremely variable. While the minimum ambient background was $0{,}06\ [nSv * h^{-1}]$, this is no representative of the base value, instead the $DR = {\sim}0{,}188 - 193{,}7\ \mu Sv * h^{-1}$ should be taken.

The following background considerations have been taken in account for the analysis of the hot-cells data in the next section:

1. Assuming the lowest value of the background at $0{,}06\ nSv/h$ from the yellow shielding box [4];
2. Evaluating an Avg. DR during the total four weeks measurements (first, second and third campaign) by the Area Radiation Monitor instruments, $Avg. DR = {\sim}0{,}188 - 193{,}7\ \mu Sv * h^{-1}$ [4]. This will be our reference min. value of DR in the area;

Few long background measurements were performed with gamma camera in different position of the hallway and with all hot-cell doors closed in front of the reference hot-cells.

The followings sub-sections will show the Gamma imaging results of 5 hot-cells analysed where for each of them gamma spectra image was superimposed onto the optical view taken for the top side and the bottom side of the cell. For some hot-cells, for better visualization, it also associated a referenced optical image to better visualize the hot-spot/s. Besides, for some of them in order to better identify and localize the hotspot, a further analysis was performed.

In the pictures the labels are created automatically by the algorithm software and for that reason sometimes do not respect the actual result of the final report in term of confidence level. Besides, all the arrows represented in the pictures and outside the red-box or the image itself should be disregard because not validate as identified radioisotopes. In some cases the software doesn't show the final result in the image (like [7]) or put a label of less than 100% confidence level, the reader should be only refer at those as a general hotspot/s position only, while the final data are in the Table 5 as they resulted from the PDF report and the post-processing of the data.

We follow the GI setup of the previous campaign [4], [7] but at the same time we improve the actual measurement positioning. The NuVISION gamma camera was set up in front (static mode) of the hot-cell at the minimum compatible distance ($8 - 131\ cm$) from the Plexiglas screen and the Plexiglas screen was removed from all the cells after the radioprotection safety conditions had been satisfied (see table below for details Table 5).

The acquisition measurement times have been set to optimize and complete the acquired data from the previous campaign [4], [7] if it was necessary to improve the data from the previous hot-cell or if the specific hot-cell was never recorded (i.e., at least full energy peak (FEP) radioisotope for a statistical error $\lesssim 5\%$).

The work-program was optimized following the guidelines of the preliminary assessment of the campaign on the basis of the information from the first and second one. The activities were following a preliminary time schedule that during the measurement campaign was adjusted in order to accomplish the best quality results possible in relation to the available time (i.e. increasing the measurement time and performing measurement at different angle of view). In the plan the two most important variable on the time schedule were the opening of the hot-cell with consequently the radioprotection verification of the radiological status and the acquisition time (item 1.2 and 1.3 in [7]). Those two tasks showed the effectively time length for each hot-cell that it was essentially shifted to about one hot-cell pro-day differently as it was previously planned.

Besides, it is important the time utilized to take the background data (green band on Figure.7 [7]) that it was optimized during the night.

For all five analysed hot-cells, when present, an identified radioisotope is showed with a radio-isotopes specific colour gradient spot (see details in Table 5). From the report [7], Cs-137 was identified in every spectrum collected and it was ranging from $1.5\ Bq \cdot cm^{-2}$ to $173\ kBq \cdot cm^{-2}$; Eu-154, Co-60 and Am-241 were also frequently seen. In our GI measurements showed practically everywhere Cs-137 radioisotope while the Am-241 was seen only in some hot-cells. This is due to the small size CZT detector that has difficulty to identify low energy gamma lines (i.e., 59keV gamma line) as well as low quantity of Eu-154 present. The Co-60 was sometimes visible but not identified by the GI (see pictures below in Figure 26), like in the hot-cell J. For all the hot-cells the hotspots localized at the border of the FOV (red dashed line) of the GI cannot be taken in account because it cannot be considered accurate (i.e. as well as the confidence level always $< 7\%$).

An interesting result is showed on the gamma spectra of the hot-cell G (Figure 24). There are slightly visible the Am-241 energy peaks $59{,}5keV$ and $26{,}3keV$ and the NuVSION software reports a dose rate of $0{,}088\ \mu Sv/h$ with 100% confidence level. Nevertheless this data should be taken with care because the level of the dose rate is close to the instrument sensitivity level ($50nSv/h$) and at the limit of CZT's efficiency at very low energy. Limitation on resolving low energy peaks could have been achieved using the GI in *low Energy mode* as it is possible in the Detection Settings of the NuVISION software. While the Cs-137 $662keV$ energy peak is also visible, the reconstruction algorithm (i.e. NuVSION software algorithm) cannot reconstruct it most likely due to the high background around it and the consequent absence of the Compton edge of the Cs-137 (see Figure 25).

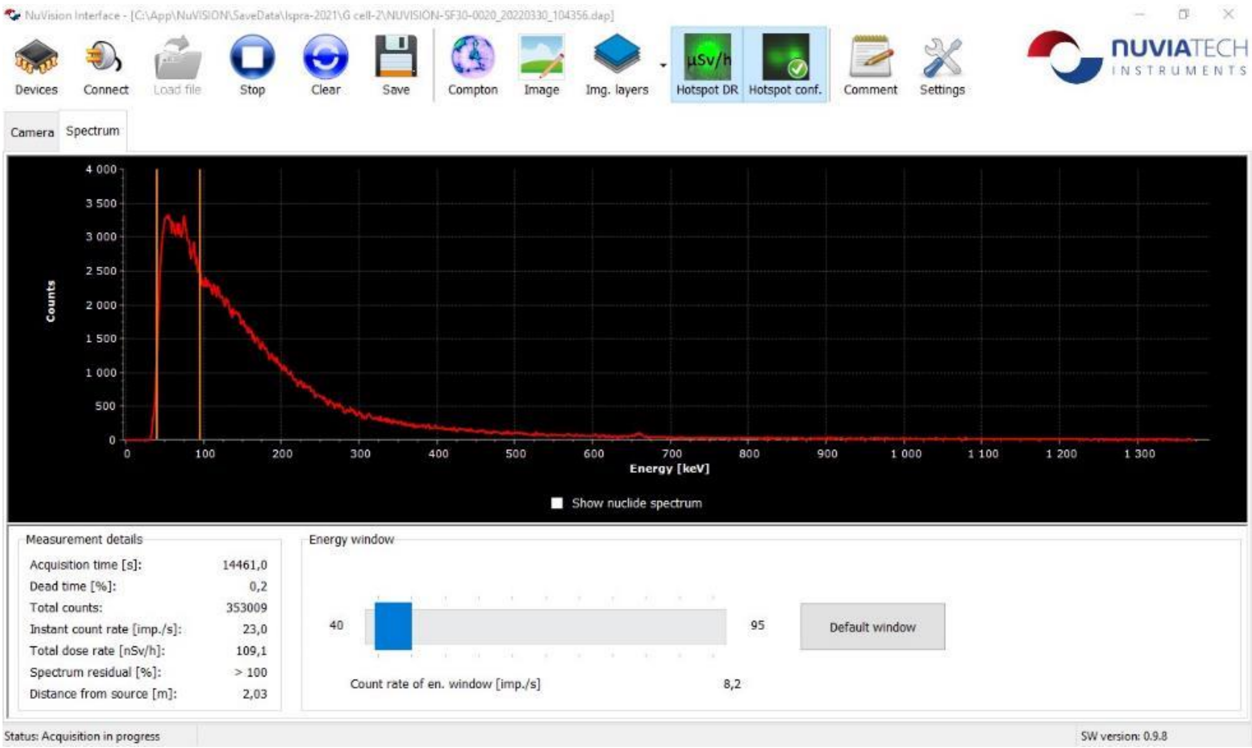

Figure 24: *Gamma spectra from the hot-cell G. The ROI is in the Am-241 energy region (linear scale).*

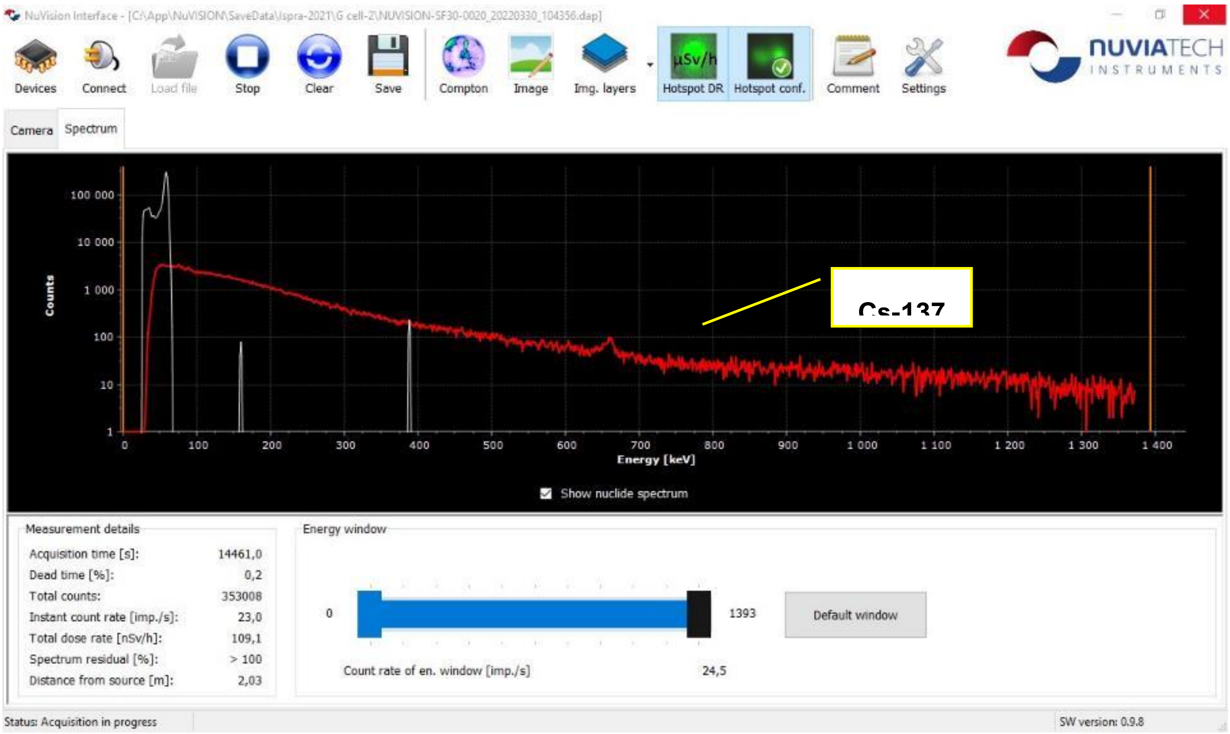

Figure 25: Gamma spectra from the hot-cell G. The reconstruction white line in the Am-241 energy region (log scale) and visible the Cs-137 energy peak.

Another interesting result is showed in the hot-cell J, where the presence of the two Co-60 energy peaks ($1{,}173$ and $1{,}332\ keV$) were already observed in the first measurement campaign [4] but due to the low acquisition time there was no identification by the NuVSION algorithm. In the current measurement on the hot-cell J, we increased the acquisition time up to $60345{,}3[sec]$ and we could see clearly the two Co-60 peaks and even the two Compton edges (see Figure 26) but still no identification by the algorithm software. It could be linked to the difficulty for the software to discern the profile of the spectra in relation to the high background or in other words to the threshold level of the signal/noise ratio.

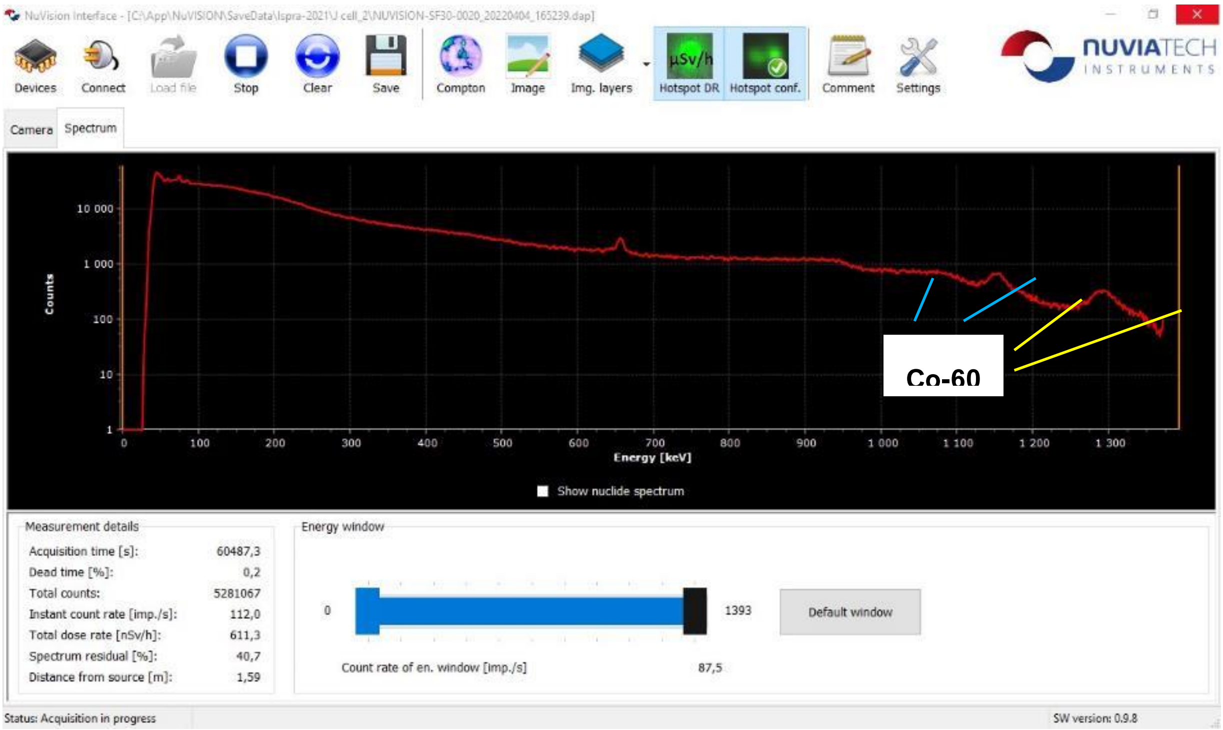

Figure 26: Gamma spectra of the hot-cell J.

Top view

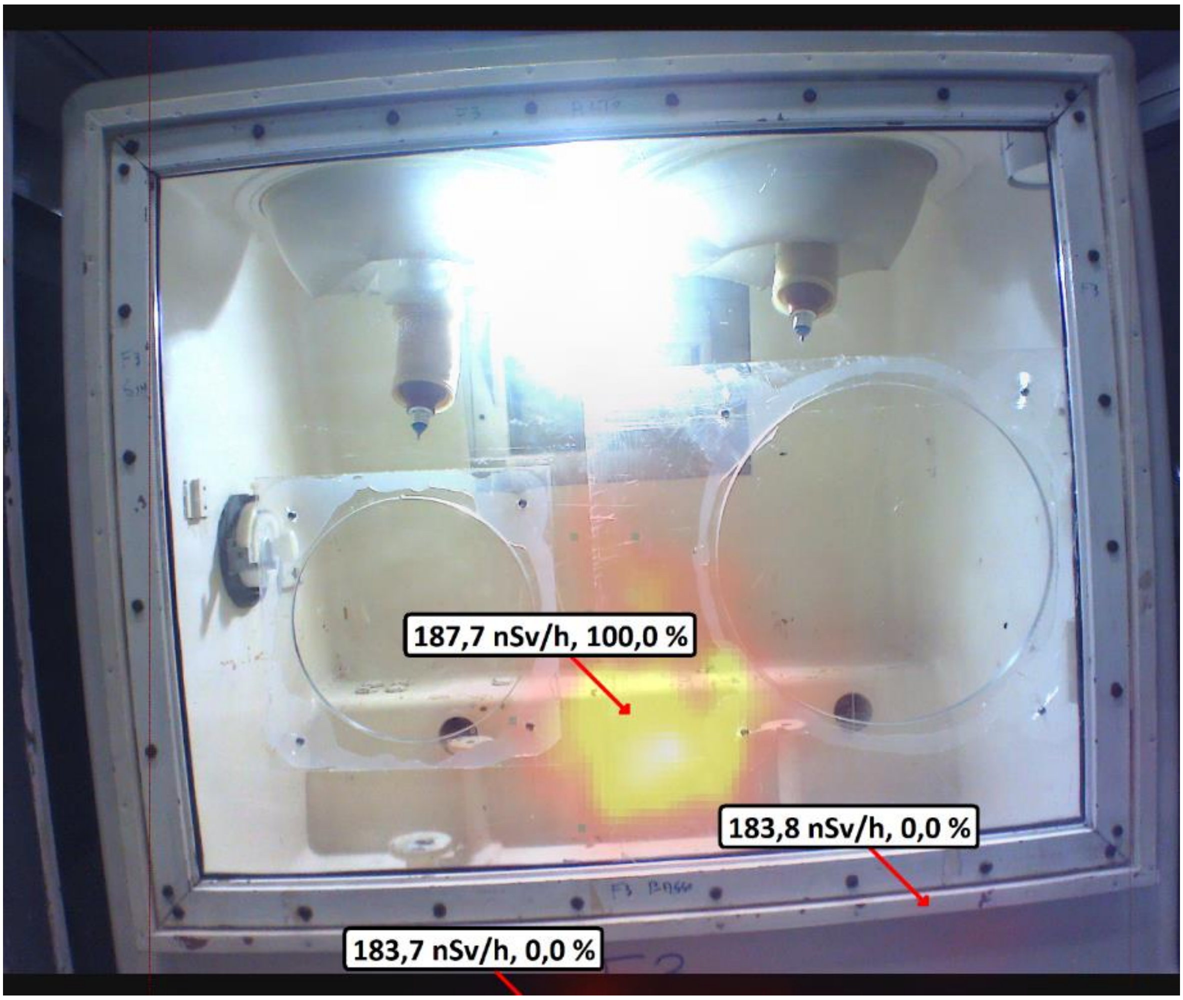

Figure 27: *Gamma camera images on hot-cell F3 (the highest dose is indicated with the lightest colour - white). Arrows outside or close to the red dashed box shouldn't be taken in account.*

Top view optical image

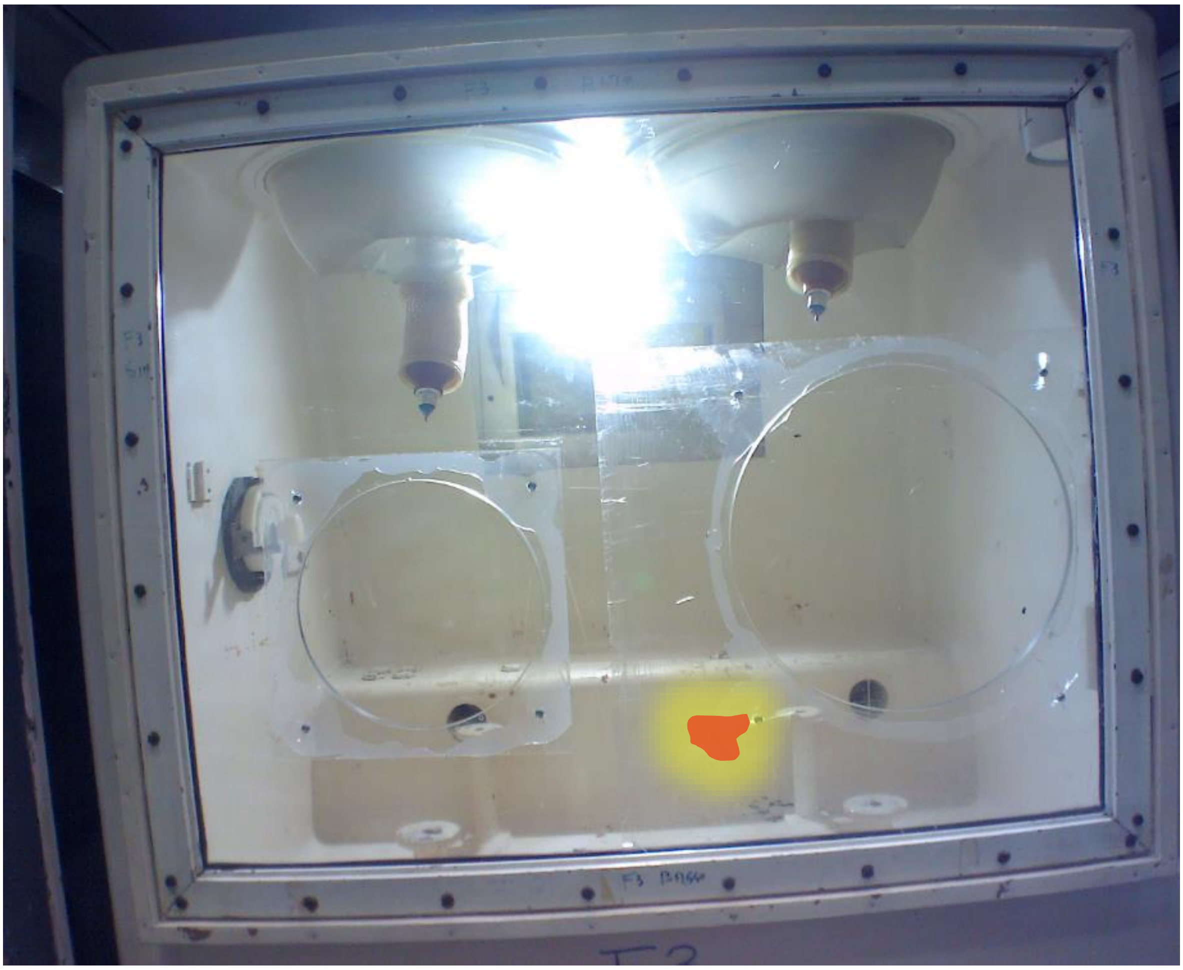

Figure 28: Gamma camera optical image on hot-cell F3 with a simple representation of the hot-spot/s

5.3. Findings and results

The scanning results of the two buildings are focused on the geo-localization quality of the data in a dynamic mode, on inside buildings and associated radiological data.

For building 52a were taken three trajectories and for building 52 were taken eight trajectories with MLSP and PGIS-2 data. Following we will describe the post processing of the data coming separately from the PGIS-2 and MLSP. After that the data are combined to obtain the results of geo-localized radiological inside the buildings 52 and 52a.

The MLSP data is processed in the STeAM Desktop software to generate the reference maps and acquisition trajectories. The following steps are carried out for each building (52 and 52a):

The longest acquisition is processed in mapping/SLAM mode, i.e. the 3D map and trajectory are generated simultaneously from the acquired LiDAR data. The map serves as reference for the remaining acquisitions and is placed in a local coordinate frame. It is also possible to align the map with an external (world) coordinate frame, however, this was not considered necessary for this exercise.

The remaining acquisitions are processed in tracking mode against the reference generated in the previous step to ensure that all trajectories are perfectly aligned in a single coordinate frame. Each trajectory contains the 3D pose (position and orientation) and corresponding timestamp (at 12 Hz) with an accuracy of approximately $2cm$. Figure 23 shows the resulting maps (projected on the 2D ground plane for better visualization) with the corresponding trajectories overlaid.

A python script was developed for merging the PGIS-2 and MLSP data based on the timestamps that are common to both datasets, i.e. it takes the timestamp for each radiation measurement and computes the associated position by linearly interpolating the poses in the corresponding MLSP trajectory. For visualization, each measurement is plotted on the 2D reference map colour-coded according to the radiation level (see Figure 29).

The MLSP and PGIS-2 data acquisition is running on two different devices (Windows tablet and android phone, respectively). To obtain an accurate data fusion, it is important to have a time-synchronization between them. In the current experiment the offset was estimated manually, however it can also be calculated using the inertial sensors that are available in both setups [6]. The data fusion also considers the geometric offset between the origin of the MLSP pose estimation (i.e. the position of the LiDAR head, see Figure 20) and the position of the nuclear detector (the nominal offset in the current setup was measured as $0.33m$ in *X* and $1.62m$ in *Y* axis).

The main limit to the localization accuracy is the fact the radiation measurement is integrated over $1\ sec$ and therefore the position uncertainty corresponds to the movement of the trolley during this time, i.e. the uncertainty increases with the speed of the trolley.

The following table shows the acquired the data from the MLSP system and the PGIS-2 device, TXT and PEI/TXT types respectively.

The two days measurement campaign concluded with a total of extracted 11 measurements acquired for dynamic geo-localization with MLSP and a NuHLS-100 RIID inside building 52 and 52a.

The final data fusion MLSP+PGIS-2 are represented on the below pictures (Figure 29) and they show the tracks for the building 52a and building 52. The associated radiological data are colour coded showing the recorded CPS by PGIS-2. If we analyse the zoom-in pictures of the respective 52a and 52 radiological tracks (lower two picture of Figure 29), we could identify for the building 52a a higher counting rate on the region of the containment radioactive box visible in the picture (bottom left of Figure 29 dashed black circle). Besides, it shows another source of higher counting rate (bottom left of Figure 29 dashed black oval) on the tank $50\ m^3$ in volume, containing low level liquid waste (LLLW). This is in agreement with a previous measurement under the INSIDER H2020 project in 2017-‘21 (Improved Nuclear SIte characterization for waste minimization in DD operations under constrained EnviRonment) that has showed very similar radiological results with different RIIDs.

In the building 52 (see Figure 29) we can identify clearly two regions of higher counting rate that are indicate in the zoom-in (bottom right picture in Figure 29) with two dashed shapes. No specific radiological attribution of those area because is out of scope of this document.

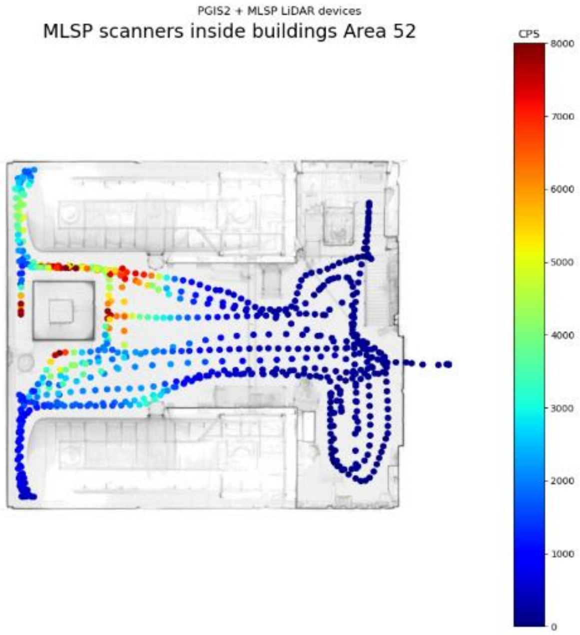

Radiological data geo-localized inside the bldg.52a

Radiological data geo-localized inside the bldg.52

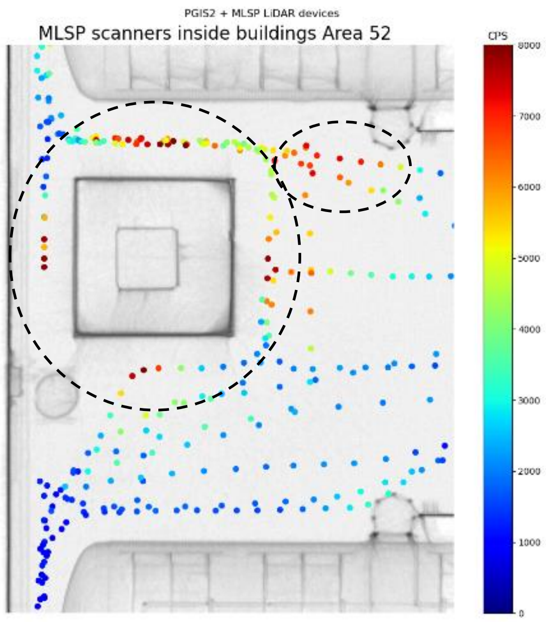

Zoom-in in bldg.52a

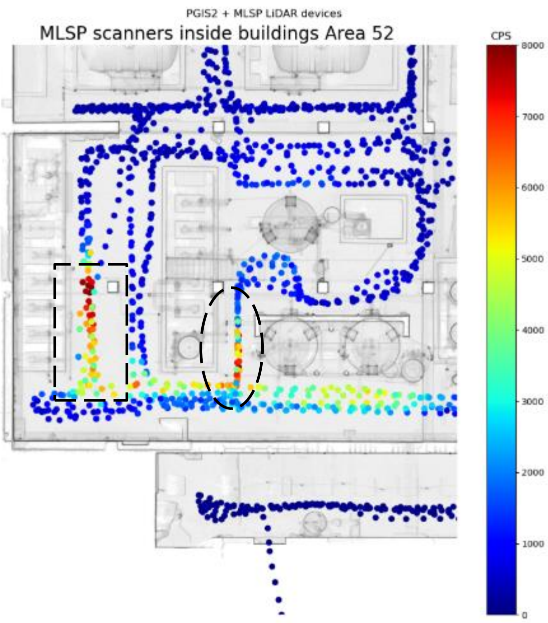

Zoom-in in bldg.52

Figure 29: Radiological data (CPS) representation after the processing of the data from MLSP and PGSI-2.

This case study demonstrated that the geo-localization with a MLSP system coupled with a radiological handheld device (NuHLS-100) could provide accurate radiological data and **geo-localisation** precision in an **inside** building up to $\sim 2cm$ if each track is performed with the following characteristics:

- PGIS-2 at a lower distance to the floor and strongly collimated;
- Slow walking pace for punctual radiological data;
- Clear FOV of the LiDAR scanner

The use of a similar system MLSP+RIID data will provide the following advantage that could be extended to different areas of the JRC-ISPRA site and more generally to other nuclear sites under decommissioning:

- Fast radiological survey of an area ($\sim\mathbf{30m^2/min}$)[17] with geo-localized dose rate and CPS data;
- Wide applicability in indoor area;
- Precise timestamp ($\sim 1sec$) determination and possibility of data post-processing;
- Easy management of the software and extraction of the data.

Admittedly, the MLSP+RIID survey technique has also some limitations:

- Limited LiDAR view in tight spaces or significant obstruction of LiDAR scanner;
- Availability of radioactive sources as reference points for accurate geo-localization and verified radiological base line;
- Longer post-processing due to a not integrate fusion software between the MLSP and the RIID;
- Inaccurate radiological position determination of the NuHLS-100 (i.e. absence of a collimator).

One of the improvement that is already in the modelling phase, will be the use of a lead shielding blanket around the PGIS-2 (see technical note [4]). This shielding should improve the determination of the radiological hot-spot/s localization by narrowing the field of view of the detector where interference from external radioactive sources could affect the results. As mentioned, and fully explained in the technical document [4] this is constituting a **limiting factor** for a precise radiological localization.

CASE with Gamma Camera

The Gamma camera proved to be a valuable instrument for fast and effective radiometric mapping/identifying preliminary characterisation of the nuclear facility components. The first campaign revealed the advantages and the limitations of the gamma camera like measurement in LCSR (e.g. fast hot-spot identification and localization, GI portability and setup configuration and more see [7] and related), the second campaign showed the possibility to improve the accuracy of the final radiological data (i.e. dose rate and hotspots identifications) and gave a better understanding of the influence of the background radiation in the area.

Here we summarize the achievements for the third campaign:

- We tested Increasing the measurement time and it consequently led to lowering the statistical error on FEP;
- New background evaluation and extra background spectra in the area;
- Improved accuracy of the hot-spots thanks to the removal of the Plexiglas screen and decrease of the distance from the GI to the identified hot-spot (like hot-cell J);
- We finalized the remaining hot-cells: F3, F4, G, K2 and J for a complete radiometric picture of the area.

---

[17] Considering a dynamic measurement at $0.75m/sec$ walking speed and a device solid angel of $\sim 1m^2$.

The results of this campaign together with data from the other two are summarized in the data chart below (Table 5) and also plotted the radiological results of the 15 hot-cells in relation to the background value of the area (see **Figure 30**). The columns:

- "*Hot-cell#*", the name in **bold** means it is measured in the third campaign and in *italic* the first and second campaign data [4], [8]
- "*Total measurement time*" indicates the Live time for each campaigns and for each hot-cell top and bottom,
- "D*ose rate*", is the dose rate (i.e. ambient dose equivalent H*(10)) calculated at the head of the detector for the *Top* and the *Bottom* part of the hot-cell (i.e. what it is defined as *Top view* and *Bottom view* in the Sec.6 [7]),
- "*Completed"*, as simple Yes/No value
- "*Notes*" are indicated the recommendations or other comments on the data for an improvement of this radiological survey with the GI.

There are few comments about the radiological results from the full campaign as mentioned in the last reports [7] and [4]:

- In the first campaign the Plexiglas wasn't removed and that interfered with the determination of the distance by LASER for the dose rate estimation at the head of the detector;
- In the first campaign the hot-cells I2 got interference from the Cs-137 background from the entrance hot-cell (higher value in comparison to the second campaign) at the end of the hallway [4] while it was shielded in the second campaign;
- In the second campaign, we increased the measurements times. Thus we improve the accuracy of the results (visible in the hot-cells A, D and F1 that had a discrepancy of $\sim 30\%$) not present in the hot-cell C where we had similar LT with only $\sim 7\%$ discrepancy;
- In the third campaign we had a background measurement for some hot-cells (all the hot-cells' doors closed) to be eventually subtracted from the specific hot-cell measurements (like for hot-cell G and K2) to show the variation of absolute cps of FEP for Cs-137.

Table 5 : *Summary of the NuVISION gamma camera of all three campaigns 2021-2022.*

Hot-cell #	**Total measurement time (s)**	**Dose rate at the camera head (µSv.h^{-1})**		**Distance[18] [m]**		**Completed**	**Notes**
		Top	*Bottom*	*Top*	*Bottom*		
A	64951	0,30	0,45	2,21	2,29	Yes	
A	19589	<0,2	NA	1,54	NA		
B	15563	0,29	0,34	2,36	2,29	Yes	

[18] NA, Not Available: for those points where the distance determination is inaccurate due to the Plexiglas presence or other technical reasons.

C	6808	0,46	NA	2,52	NA	Yes	Large hot-cell
C	6902	0,49	NA	NA	NA		
D	13404	0,26	0,33	2,63	2,18	Yes	
D	2450	<0,2	NA	NA	NA		
E	2005	0,32	Na	1,85	NA	Yes	
F1	6028	0,31	0,35	2,09	1,97	Yes	
F1	2416	<0,2	NA	NA	NA		
F2	66482	1,35	1,00	2,45	2,23	Yes	values only after the cleaning from RPO
F2	1912	1,10	NA	NA	NA		
F3	2407	0,36	0,36	NA	2,37	Yes	
F3	85404	0,21	0,23	1,18	1,50	Yes	
F4	2891	0,45	0,40	NA	1,98	Yes	
F4	82779	<0,2	<0,2	1,08	2,31	Yes	
G	3023	0,53	0,53	NA	1,42	Yes	
G	14437	<0,2	NA	2,03	NA	Yes	
H	66602	0,49	NA	1,82	NA	Yes	
I2	81012	1,10	3,70	1,74	2,09	Yes	
I2	2232	3,00	3,00	NA	2,28		
J2	5216	0,82	0,81	1,49	1,49	Yes	investigate the identification of Co-60
J	63719	1,80	NA	1,21	NA	Yes	Large hot-cell
K1	22526	0,38	0,41	2,63	2,27	Yes	
K2	80917	<0,2	NA	1,93	NA	Yes	Large hot-cell
Background[19]	581670	0,06 < to < 0,20		NA		No	more GI positions

[19] This is the background variation of the full campaign by the GI.

The following plot (see Figure 30) shows the radiological distribution acquired from the GI during the five weeks measurement campaign on 15 hot-cells in LCSR. The red dashed line is the average recorded background by the Area Radiation Monitor ($\sim 0{,}188\ [\mu Sv * h^{-1}]$ reference background value). It is clear that most of the hot-cells (five out of fifteen hot-cells) have very close dose rate values to the background (considering a 20% uncertainty on the gamma GI data). Except for the hot-cells F2, I2 and J where we see an increase by factors of $3.4, 4.2$ and 5.6 respectively to the $\sim 0{,}32\ [\mu Sv * h^{-1}]$ dose rate average of the other hot-cells. The second plot Figure 31 shows the background variation in the hallway. The red line represents the minimum background dose rate when the GI was inside the lead yellow box (see [7]-B). Two considerations about this plot:

1. The background dose rate is below $200\ [nSv * h^{-1}]$ that is the sensitivity limit of the GI;
2. The plotted data are taken during the full campaign and conditions in the area have been not always constant (drums present in the first campaign [4]).

If we assume the same conditions in the hallway, it means we consider only the background measurements taken on the third campaign (i.e., hot-cell G and K2), we could scale those two cell dose rates and we will find that both of them have essentially $DR \sim 0{,}08$. The remaining hot-cells should have also a background evaluation at the cell (all lead doors closed) and in particular for the hot-cells F2, I2 and J where there is a significantly high DR.

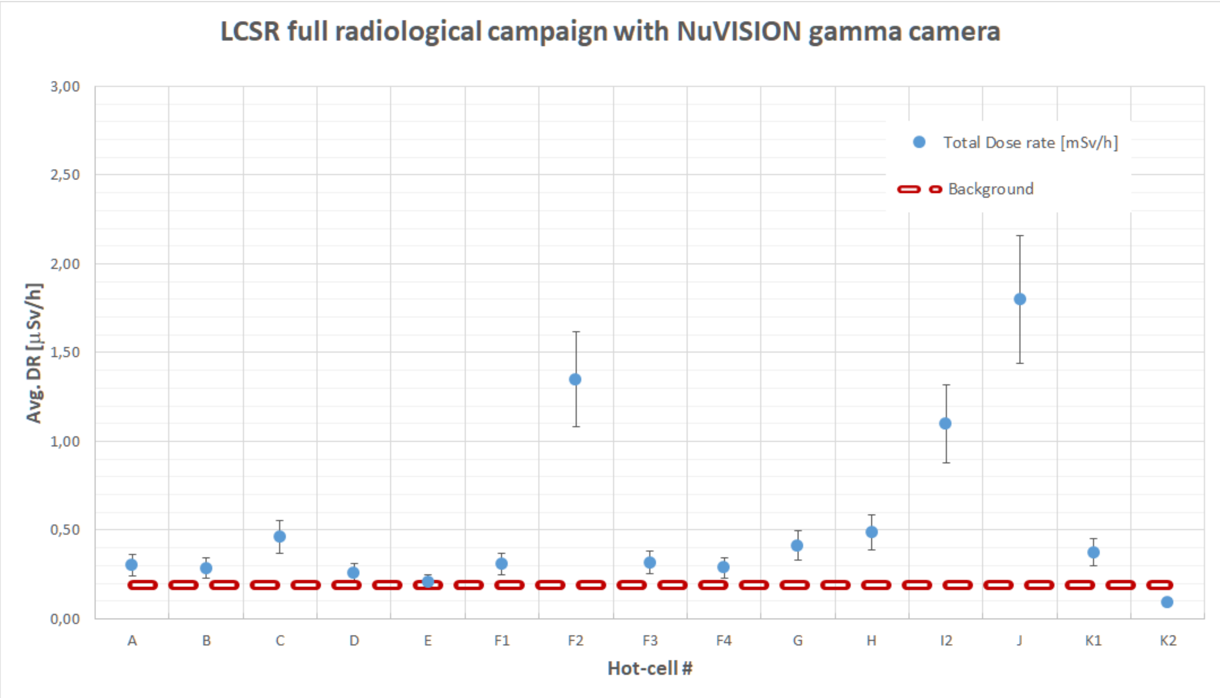

Figure 30: Distribution of the radiological response from the gamma camera in LCSR in the all three measurements campaign.

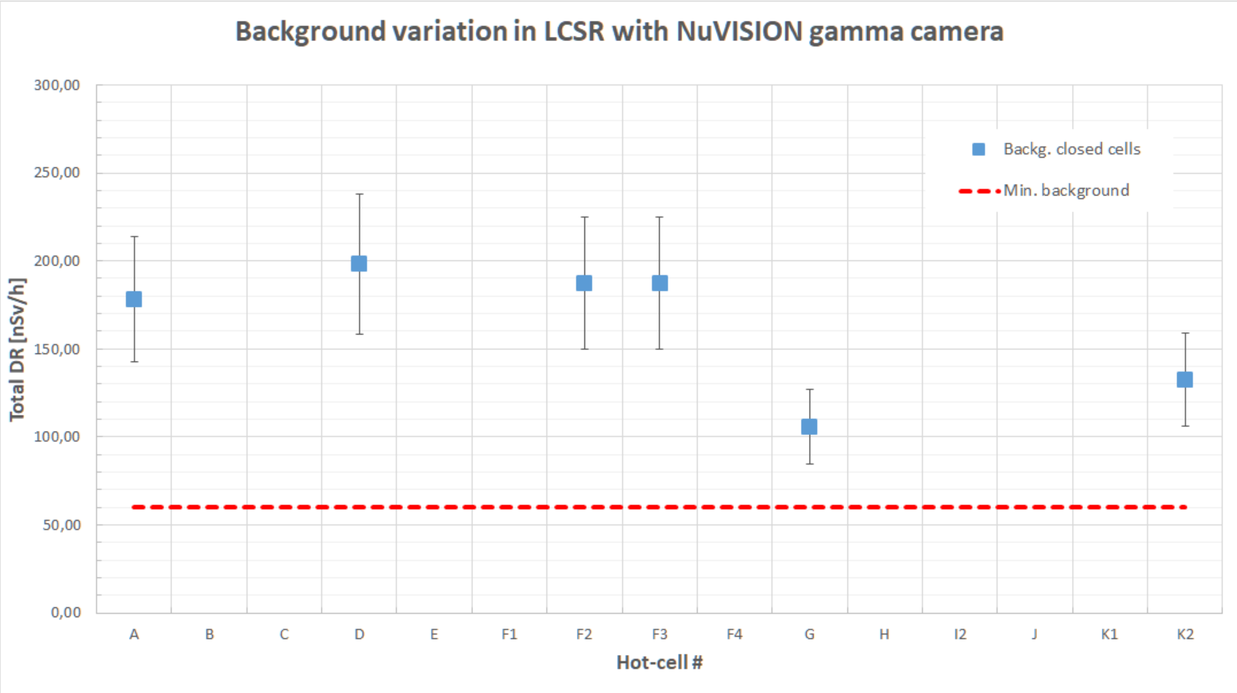

Figure 31: Distribution of the background in the hallway.

5.4. Potential Benefits for Other Organizations

The application of this case study could produce the following benefits:

- Time efficiency
- Cost workdays

6. SUMMARY

6.1. General Conclusions and Recommendation

Highlights the importance of addressing the characterisation of the site from different angles and with different approaches concerning the availability and/or experience of the operator team. One can summarise the following:

- Innovative technologies have their maximum benefit when they are applied by an expert team with deep knowledge of their characteristics to perform an efficient and effective job;
- Innovative technologies require a detailed and prepared analysis of the area's materials, type, and size to be analysed so as not to adapt the plan on the field or limit its limitations.
- They require the choice of the right tools for the specific task without assuming that one technology fits all.
- A *priori*, these innovative technologies could produce faster results and with high quality, but due to their novelty, they might not present a specific adaptability of the facility and might require a particular type of authorization.

6.2. Lessons Learned

The two case studies applied to a nuclear power plant have shown the following:

- Application of dynamic or static measurement can be achieved with other tools already used in this environment and scope (e.g., nuclear security, safety and safeguards, or emergency response).
- Their innovative solution presents few difficulties in their application due to the complexity of the use of these nuclear devices and specialised software analysis, no standard procedure available for facility characterisation with these nuclear instrumentations and lack of knowledge in automatic aerial systems in the decommissioning field.
- A mandatory definition of the planning of the radiological measurements after a detailed analysis of the environment's condition and the size of the target area.
- Achieving relevant accuracy on geo-localized radiological measurement in an inside or outside area.
- Gamma imaging system are heavily used in nuclear security for their friendly usage and very intuitive responses for an immediate assessment. In nuclear decommissioning I don't have evidence of their extended use.

In line with the above lesson learning, the quality of the radiological measurements was improved by applying learning in the field and trying to give the first analysis of the registered data on the spot. Doing that, we applied the following:

- Redefine the flight plan for the automatic (UAV+payload) and semi-automatic system (NUVISION or NuHLS-100 coupled with GNSS).
- Define the new area and time for recording radiological and GPS data.
- Optimise the time on the flight and the walking path of both systems (UAS and NuHLS-100)
- Recognize the efficiency limitation of the different type/size of the used nuclear devices.
- Gamma imaging provided an immediate visualization of the radiological status of the hot-cells. The radiological characterisation was applied without any previous preparation of the structure in study (Plexiglas was left on) and an operator could verify on the screen the presence of any gamma radiation.
- For gamma imaging analysis is a *sine qua non* condition to do a background assessment of the area around the nuclear detector as it was applied in the last set of measurement.

The registered data were completed in terms of quality assessment of the radiological characterization, and they achieved a quantifiable accuracy in geo-localization. However, they also showed their complexity of analysis. This last consideration will constrain their applicability in a "standard" (not specific as in-house technical experts at JRC-Ispra) nuclear decommissioning site.

The following table summarized few characteristics of applicability of the described case studies in nuclear decommissioning

Table 6: *Characteristics of different nuclear detection devices.*

Type of detection device	Load system	Geo-localization capability	Personnel	Absolute efficiency at Cs-137	Rugged environment	Cost/time	Technology used on decommissioning field
CZT	UAV, robot, backpack	Possible Integration with GNSS system	1 specialized technician + 1 technician	0.8 - 2%[20]	Yes, easily embedded in durable case and small size. Possibility to have a low grade of water resistance IP40	NA, detector cost ~5000€	Yes
Plastic Scintillator	UAV, robot, backpack	Possible Integration with GNSS system	1 specialized technician+ 1 technician	25-30%	Yes, easily embedded in durable case with different shape and size	NA, BC408 1500$	Yes
NaI	UAV, robot, backpack	Possible Integration with GNSS system	1 specialized technician+ 1 technician	25-30%	No, the crystal could be easily damaged and its sensitive to water	NA, ~4000$	Yes
HPGe	NA	Possible Integration with GNSS system	1 specialized technician+ 1 technician	20%	No, the crystal could be easily damaged. Standardize size	NA, ~40k$ (electrical cooled)	Yes

[20] Highly dependent on detector size

7. ANNEX 1 – Technical Specification

In this section are collected all technical specifications of the two case studies.

***Table 7**: Characteristics of the nuclear detector NuHLS-GHJP-100 and U-Blox system.*

NuHLS-GHP-100	U-Blox C099-F9P-1-03
▪ 3x3“ NaI(Tl) detector ▪ 45cm x 20cm x 15cm; 5kg ▪ Energy resolution <8.5% @ 662keV Cs-137 ▪ ADC 256/512/1024 channels (physically 8192 channels) ▪ Detection energy ranges from 20keV to 3MeV ▪ Dose rate measurement ranging from 50nGy – 30µGy/h ▪ built-in GPS receivers & Developed for Android based device ▪ Export to KMZ format direct after measurement and data presentation in Google Map ▪ Wireless Bluetooth connection between detector and Control Unit ▪ Build-in high-capacity Polymer Li-ion battery 7.4V/9Ah, full operation more than 12h ▪ Fastrax UP501 GPS receiver module with embedded GPS antenna (internal antenna) ▪ Samsung S5 device (portable antenna)	▪ ZED-F9P-04B-01 module provides dual-frequency, multi-constellation GNSS reception supporting: GPS, GLONASS, Galileo and BeiDou. In addition to the internal standalone Single Point Positioning solution, it comes with built-in RTK technology providing centimetre level accuracy to users. ▪ ZED-F9P-04B-01 module form factor of 17.0 x 22.0 x 2.4 mm ▪ GNSS acquisition cold start 25s, Sensitivity Tracking and nav. -167dBm, Nav. update rate 5Hz ▪ ZED-F9P supported protocols: UBX, NMEA 4.11 (default), 4.10, 4.0, 2.3, and 2.1, RTCM 3.3, SPARTN 2.0.1 ▪ UART baud rate 9600 - 921600 bit/s ▪ ODIN-W2 short range module for connectivity ▪ ANN-MB series, L1/L2 multi-band, high precision GNSS antenna ▪ Power supply: 2.1 mm plug 6 V-12 V DC, USB connection or LiPo cell JST connector

HERON® MS TWIN

Product Specifications

MAIN FEATURES

Suitable environment	indoor/outdoor
Handheld	possible (1)
Wearable	yes
Mountable on various mobile platforms (car, trolley, bike, quad, boat)	yes
No limits SLAM post-processing software included (HERON Desktop)	yes
Point cloud advanced processing software included (Reconstructor)	yes
Free software for x-ray maps visualization and measuring included (GoBlueprint)	yes
Output data	.e57, .las, .ply, export to ReCap
Points per second	600.000
Local accuracy	~ 3 cm
Max survey resolution	~ 2 cm
Global accuracy	~ 5 cm in short close rings (2)
Control points	yes (optional add-on)
Global accuracy with control points	~ 3 cm
Loop closure	not mandatory
Usable in every light conditions	yes
Initialization and calibration procedures	not required
Single operator	yes
Sensors working hours (in continuous acquisition)	~ 5 h
Real-time 3D point cloud visualization	yes
Real-time change detection & Automatic self-localization	yes (optional add-on)
Operating temperature	-10° ; +45°
Storage temperature	-40° ; +60°
Rugged transport case	yes

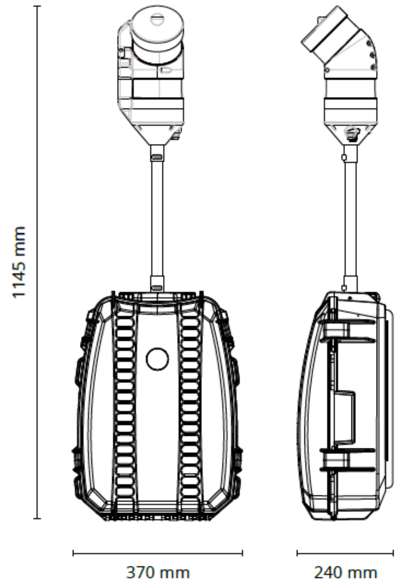

CAPTURE HEAD (REMOVABLE)

Laser sensor brand and type	Velodyne Puck LITE
No. of sensors	2
Laser safety classification	class 1
Laser wave length	903 nm
Laser max range	100 m
FOV	360° x 360°
IMU	yes
Weight	1826 g
Dimension	325 x 140 mm

SYSTEM BATTERY

Type	Li-ion battery
Capacity	12-24V / 3A / 83Wh
Weight	430 g

RUGGED TOUCHSCREEN CONTROL UNIT

Processor	Intel® Core™ i7
Weight	1200 g
Dimension	277 x 195 x 24 mm
Storage and Memory	256 GB
Protection index	IP65
Shoulder harness	282 g
Display	10.1" IPS TFT LCD WUXGA
Capacitive	Multi-touch screen
Sunlight readable technology	1000 nits LumiBond®
Power	Li-ion battery
Battery working hours	~ 2 h

www.gexcel.it

GEXCEL GEOMATICS & EXCELLENCE

Figure 32: *HERON-MS-TWIN_DATASHEET (source Gexcel)*

Table 8: *NuVISION technical specifications.*

NuVISION
▪ Size: 10x10x24 cm ▪ Weight: 3kg ▪ Detection volume: 9.6cm3 ▪ Angular Resol.: 3.5” Coded Apert., 15° Compton ▪ FoV: 45° Coded Apert., 360° Compton ▪ Battery operation: Yes (15V/5.6W) ▪ Energy range: 20-1400 keV ▪ Dose range: 1nSv/h 100mSv/h ▪ Sensitivity ^{137}Co: 50nSv/h <60s ▪ Sensitivity ^{60}Co: 50nSv/h <1s ▪ Energy res.: 2.5% at 122keV, 1.5% at 662Kev ▪ Isotope: ○ Am-341 180 cps (µSv/h) ○ Cs-137 280 cps (µSv/h) ○ Co-60 160 cps (µSv/h)

Table 9: *Gamma Camera technical specifications (Technical specifications, Low, medium and high energy mode and NuVSION software).*

Specifications	
Size	10x10x24
Weight	3Kg
Detection Vol.	9,6 cm^3 (56 grams)
Angular Resol.	3.5° Coded Apert. 15° Compton
Field of view	45° Coded Apert. 360° Compton
Battery operation	Yes (15V/6.5W)
Energy Range	20-1400 keV
Doser Range	1nSv/h-100mSv/h
Sensitivity ^{137}CS	50nSv/h < 60s
Sensitivity ^{57}CO	50nSv/h < 1s
Energy Res.	2.5% at 122 keV 1.5% at 662 keV

Isotope	c.s-1/ (µSv/h)
Am-241	1800
Cs-137	280
Co-60	160

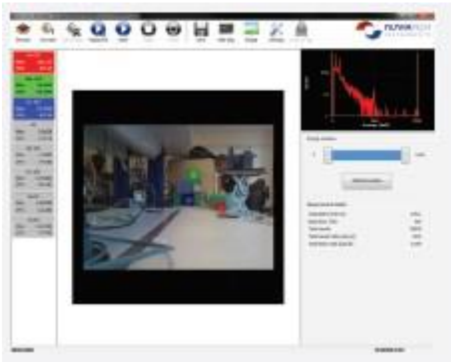

Feedback Form

FOR THE READER: if you want to provide a feedback about this knowledge product refer to this QR code and fill the linked feedback form.

8. REFERENCES

[1] Štefula, Vladan and HUBERT, Philippe, 'Pilot Project Plan – Contaminated Soil Management'. JRC-Ispra, Jun. 03, 2020.

[2] TIMOSSI, Paolo, 'Safe conservation, post operational clean out and pre-decommissioning support service to INE nuclear plant and LCSR hot-cells facility.', Directorate J - Nuclear Decommissioning and Waste Management, JRC-ISPRA, Specific offer NE.45.2802.A.023, Apr. 2021.

[3] J. DUBOSQ, 'STRRL (Area 52) Land Area Characterization Survey Report', JRC-NFD&SO, Technical note 114041_SC11_NT 04, Sep. 2016.

[4] F. Raiola, 'NuVISION GAMMA CAMERA MEASUREMENTS AT LCSR', technical note 114041_SC64_NT 02, Sep. 2021.

[5] F. Raiola, 'DYNAMIC GNSS GEOLOCALITATION OF A RADIOLOGICAL SURVEY IN AREA 52', Directorate J - Nuclear Decommissioning and Waste Management, JRC-ISPRA, technical note 114041_SC59_NT07, May 2022.

[6] F. Raiola, 'RADIOLOGICAL AERIAL CHARACTERITATION AT STRRL', NDU, JRC-ISPRA, Technical note 114041_SC59_NT05, Sep. 2021.

[7] F. Raiola, 'THIRD SERIES OF NuVISION GAMMA CAMERA RADIOLOGICAL MEASUREMENTS AT LCSR', Directorate J - Nuclear Decommissioning and Waste Management, JRC Ispra, Technical note 114041_SC64_NT 04, Oct. 2022.

[8] F. Raiola, 'SECOND SERIES OF NuVISION GAMMA CAMERA RADIOLOGICAL MEASUREMENTS AT LCSR', Directorate J - Nuclear Decommissioning and Waste Management, JRC Ispra, Technical note 114041_SC64_NT 03, Oct. 2022.

[9] 'COMMISSION IMPLEMENTING REGULATION (EU) 2019/ 947 - of 24 May 2019 - on the rules and procedures for the operation of unmanned aircraft'.

[10] 'COMMISSION DELEGATED REGULATION (EU) 2019/ 945 - of 12 March 2019 - on unmanned aircraft systems and on third-country operators of unmanned aircraft systems'.

[11] NDU, 'AREA 52 - planimetria'.

[12] NDU, 'Cisterna esterna in Area 52'.

[13] ANN/WES, 'Smantellamento parziale della STRRL del CCR di Ispra - Documentazione tecnica per l'istanza di richiesta di modifica di impianto', JRC-NFD&SO, JRC-ISPRA, Activity programme NE.20.2120.AW.004.

[14] *IAEA nuclear safety and security glossary: terminology used in nuclear safety, nuclear security, radiation protection and emergency preparedness and response*, 2022 (Interim) Edition. Vienna: International Atomic Energy Agency, 2022.

[15] *Guidelines for radioelement mapping using gamma ray spectrometry data*. Vienna: International Atomic Energy Agency, 2003.

[16] P. Hubert, 'SCTS - Contaminated soil Management'. Jun. 05, 2020.

[17] 'NEO-M8U_DataSheet_UBX-15015679.pdf'.

[18] 'NUVIA_Dynamics - RADAqLite - Release 1.30 - Final.pdf'.

[19] NDFM unit, 'Edificio 52, plant drawing'. DIR J, Mar. 07, 2006.

[20] 'Regolamento_UAS-IT080121.pdf'.

[21] N. Vaughan and B. Gabrys, ‘Comparing and Combining Time Series Trajectories Using Dynamic Time Warping’, *Procedia Comput. Sci.*, vol. 96, pp. 465–474, 2016, doi: 10.1016/j.procs.2016.08.106.

[22] ‘European Commission. Joint Research Centre. - 2018 - Sensor Tracking and Mapping (STeAM)..pdf’.

[23] S. Ceriani, C. Sanchez, P. Taddei, E. Wolfart, and V. Sequeira, ‘Pose interpolation SLAM for large maps using moving 3D sensors’, in *2015 IEEE/RSJ International Conference on Intelligent Robots and Systems (IROS)*, Hamburg, Germany: IEEE, Sep. 2015, pp. 750–757. doi: 10.1109/IROS.2015.7353456.

[24] European Commission. Joint Research Centre., *Sensor Tracking and Mapping (STeAM).* LU: Publications Office, 2018. Accessed: Apr. 09, 2024. [Online]. Available: https://data.europa.eu/doi/10.2760/762493